

# PONTE SULLO STRETTO DI MESSINA



## PROGETTO DEFINITIVO

### EUROLINK S.C.p.A.

IMPREGILO S.p.A. (MANDATARIA)

SOCIETÀ ITALIANA PER CONDOTTE D'ACQUA S.p.A. (MANDANTE)

COOPERATIVA MURATORI E CEMENTISTI - C.M.C. DI RAVENNA SOC. COOP. A.R.L. (MANDANTE)

SACYR S.A.U. (MANDANTE)

ISHIKAWAJIMA - HARIMA HEAVY INDUSTRIES CO. LTD (MANDANTE)

A.C.I. S.C.P.A. - CONSORZIO STABILE (MANDANTE)

#### IL PROGETTISTA

**COWI**

Ing. E.M. Veje  
Dott. Ing. E. Pagani  
Ordine Ingegneri Milano  
n° 15408



#### IL CONTRAENTE GENERALE

Project Manager  
(Ing. P.P. Marcheselli)

#### STRETTO DI MESSINA

Direttore Generale e  
RUP Validazione  
(Ing. G. Fiammenghi)

#### STRETTO DI MESSINA

Amministratore Delegato  
(Dott. P. Ciucci)

Unità Funzionale

OPERA DI ATTRAVERSAMENTO

PB0035\_F0

Tipo di sistema

STUDI DI BASE

Raggruppamento di opere/attività

STUDI AERODINAMICO (ANALITICI E SPERIMENTALI)

Opera - tratto d'opera - parte d'opera

Basic Studies

Titolo del documento

Wind Tunnel Tests, Cables



CODICE

C G 1 0 0 0 P R G D P S B S 3 0 0 0 0 0 0 0 3 F0

REV	DATA	DESCRIZIONE	REDATTO	VERIFICATO	APPROVATO
F0	20/06/2011	EMISSIONE FINALE	ALN	SAMI	ALN/EYA

NOME DEL FILE: PB0035\_F0





		<b>Ponte sullo Stretto di Messina</b> <b>PROGETTO DEFINITIVO</b>		
Wind Tunnel Tests, Cables		<i>Codice documento</i> PB0035_F0.docx	<i>Rev</i> F0	<i>Data</i> 20/06/2011

## INDICE

INDICE .....	3
1 Executive summary.....	5
2 Sub-tests C1 .....	5
2.1 High Reynolds' Number tests.....	5
2.2 Model set-up and measurements.....	6
3 Key Results.....	7
4 Conclusions .....	10
5 References .....	11
Appendix - Scope of Work .....	12



		<b>Ponte sullo Stretto di Messina</b> <b>PROGETTO DEFINITIVO</b>		
Wind Tunnel Tests, Cables		<i>Codice documento</i> PB0035_F0.docx	<i>Rev</i> F0	<i>Data</i> 20/06/2011

## 1 Executive summary

This report describes wind tunnel tests carried out with the objective of acquiring wind load coefficients for the twin main cable configuration of the Messina Bridge and to make a qualitative assessment of the risk for galloping instability of the back stays.

The wind tunnel tests are motivated by the fact that representative data for the twin cable element configuration is not available for sufficiently high Reynolds' Numbers required to be representative for the SILS condition.

The result of the tests shows that the wind load coefficients representative for the twin cable elements is substantially different from coefficients valid for low Reynolds' Numbers available in the literature. Further the tests indicates two potential galloping type instabilities for the bridge back stays.

## 2 Sub-tests C1

The main cable sub-tests C1 were carried out at the high pressure wind tunnel at DLR, Göttingen, Germany. The scope of work for the C1 sub-tests is enclosed in Appendix 1.

### 2.1 High Reynolds' Number tests

The Reynolds Number,  $Re$ , of a cylindrical structure is defined in terms of the cylinder diameter  $d$ , the onset flow speed  $V$ , the dynamic viscosity  $\mu$  and the fluid density  $\rho$ :

$$Re = \frac{\rho d V}{\mu} = \frac{d V}{\nu}$$

The ratio  $\nu = \mu/\rho$  is the kinematic viscosity which often is assigned the value  $\nu = 1.5 \cdot 10^{-5} \text{ m}^2/\text{s}$  for wind engineering applications. The dynamic viscosity of atmospheric air can be considered independent of ambient pressure but is a weak function of temperature and at  $20^\circ \text{C}$   $\mu \approx 1.8 \cdot 10^{-5} \text{ kg/m}\cdot\text{s}$ . The density of atmospheric air is also a weak function of temperature and proportional to the ambient pressure. At atmospheric conditions and at  $20^\circ \text{C}$  the dynamic density is  $\rho \approx 1.2 \text{ kg/m}^3$ .

For the main cable elements of the Messina Bridge at the SLIS condition the full scale Reynolds' Number is obtained as  $Re \approx 1.2 \text{ m} \cdot 70 \text{ m/s} / 1.5 \cdot 10^{-5} \text{ m}^2/\text{s} = 5.6 \cdot 10^6$ . It is difficult to obtain such high  $Re$  in a conventional ambient pressure wind tunnel unless the tunnel is very large and can

		<b>Ponte sullo Stretto di Messina</b> <b>PROGETTO DEFINITIVO</b>		
Wind Tunnel Tests, Cables		<i>Codice documento</i> PB0035_F0.docx	<i>Rev</i> F0	<i>Data</i> 20/06/2011



accommodate over size models. By increasing the ambient pressure in the wind tunnel over the atmospheric pressure it is possible to obtain very high  $Re$  even with small models. For the present tests the pressurized wind tunnel at DLR was operated up to a pressure of approximately 80 bar and at a maximum wind speed  $V = 35$  m/s. With a model cylinder diameter of  $d = 0.038$  m this yielded a maximum Reynolds' Number  $Re \approx 80 \cdot 1.2 \text{ kg/m}^3 \cdot 0.038 \text{ m} \cdot 35 \text{ m/s} / 1.8 \cdot 10^{-5} \text{ kg/m} \cdot \text{s} = 7 \cdot 10^6$  accommodating full scale Reynolds' Numbers.

## 2.2 Model set-up and measurements

The tests were carried out with a model consisting of two aluminium cylinders mounted with parallel axes perpendicular to the flow at a distance of  $1.57 \cdot d$ . The cylinders were polished to a relative surface roughness  $k/d \approx 10^{-5}$  modelling approximately the anticipated surface roughness of cableguard wrapping. One of the cylinders was fixed to the side walls of the measurement section while the other cylinder was at each end attached to a strain gauge force balance, which allowed the lift and drag forces to be measured in directions perpendicular and parallel to the flow. The strain gauge balance was mounted on a turn table such that the position of the instrumented cylinder could be shifted to be in upwind and downwind positions relative to the stationary cylinder. A view of the twin cylinder set up in the removable test section is shown in Figure 2.1.



Figure 2.1 Twin cylinder model of main cable set-up in the DLR pressurized wind tunnel.

		<b>Ponte sullo Stretto di Messina</b> <b>PROGETTO DEFINITIVO</b>		
Wind Tunnel Tests, Cables		<i>Codice documento</i> PB0035_F0.docx	<i>Rev</i> F0	<i>Data</i> 20/06/2011

The measurements proceeded by first setting the wind tunnel ambient pressure. Then the instrumented cylinder was located upwind of the fixed cylinder, the wind speed was set and the forces were measured at inflow angles spanning the range of  $-24 \text{ deg} < \alpha < 24 \text{ deg}$  with horizontal in increments of 2 deg. Upon completion of the upwind position the instrumented cylinder was moved to the downwind position and measurements in the  $-20 \text{ deg} < \alpha < 20 \text{ deg}$  interval was repeated. This procedure was repeated for a set of preset wind speeds and for ambient pressures of 20, 40, 60 and 80 bar thus spanning a Reynolds Number range of  $1.5 \cdot 10^5 < Re < 7 \cdot 10^6$ .

A detailed account of the measurements and results are given in [1].

### 3 Key Results

The measured mean lift and drag forces  $F_{L,D}$  acting on the instrumented cylinder model were made non-dimensional through normalisation with the dynamic head  $\frac{1}{2}\rho V^2$ , model span length  $L_A$  and model diameter  $d$  to yield the lift and drag coefficients  $C_L$ ,  $C_D$ :

$$C_{L,D} = \frac{F_{L,D}}{\frac{1}{2}\rho V^2 L_A d}$$

The sign convention adopted in [1] and the present report is shown in Figure 3.1.

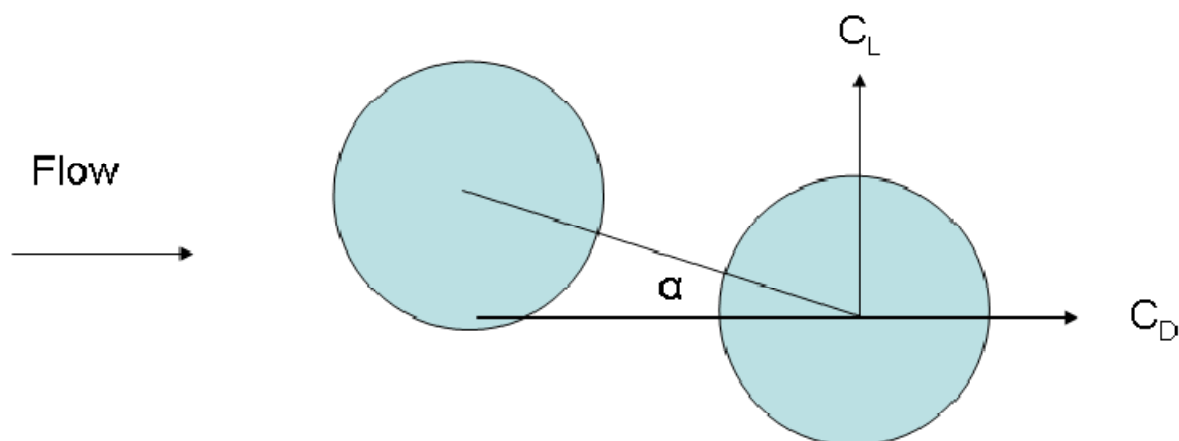




Figure 3.1 Sign convention for lift, drag and angle of attack adopted in the present study

The key results are presented as the drag coefficients of the upwind cylinder ( $C_{D1}$ ) and downwind cylinder ( $C_{D2}$ ) as function of Reynolds' Number for flow in the plane of the two cylinders (i.e.  $\alpha = 0$ )

		<b>Ponte sullo Stretto di Messina</b> <b>PROGETTO DEFINITIVO</b>		
Wind Tunnel Tests, Cables		<i>Codice documento</i> PB0035_F0.docx	<i>Rev</i> F0	<i>Data</i> 20/06/2011

deg.), Figure 3.2 and the lift coefficient of the downwind cylinder as function of inflow angle  $\alpha$ , Figure 3.3.

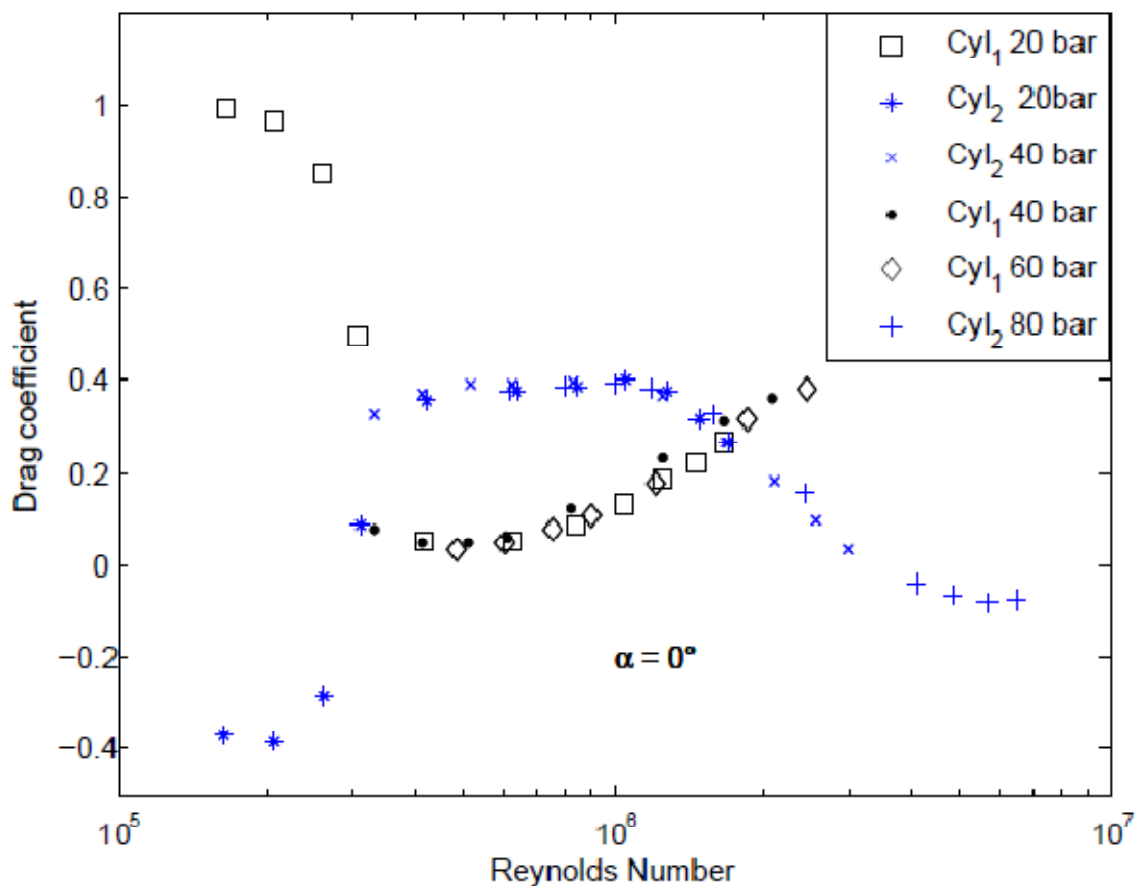




Figure 3.2 Drag coefficient of upwind (Cyl<sub>1</sub>) and downwind cylinder (Cyl<sub>2</sub>) as function of Re for flow in the plane of the two cylinders ( $\alpha = 0$  deg).

From Figure 3.2 it is noted that the drag coefficient of the upwind cable element (Cyl<sub>1</sub>) assumes values of  $C_D \approx 1$  for sub-critical Re ( $Re < 3 \cdot 10^5$ ). In the critical range  $C_D \approx 0$  indicating almost no wind loading on the upwind cable element whereas  $C_D$  increases again in the super-critical range. It was not possible to extend the  $C_D$  measurements beyond  $Re \approx 2 \cdot 10^6$  due to severe vortex shedding vibrations. The asymptotic value of the drag coefficient at the high Re plateau is however expected to be at  $C_D = 0.5$  based on the well known ratio for single isolated cylinders. For the downwind cable element the trend is reversed beginning with  $C_D \approx -0.4$  (suction) at sub-critical Re and ending asymptotically at  $C_D \approx -0.1$  for super-critical Reynolds' Numbers,  $Re \approx 7 \cdot 10^6$ .



		<b>Ponte sullo Stretto di Messina</b> <b>PROGETTO DEFINITIVO</b>		
Wind Tunnel Tests, Cables		<i>Codice documento</i> PB0035_F0.docx	<i>Rev</i> F0	<i>Data</i> 20/06/2011

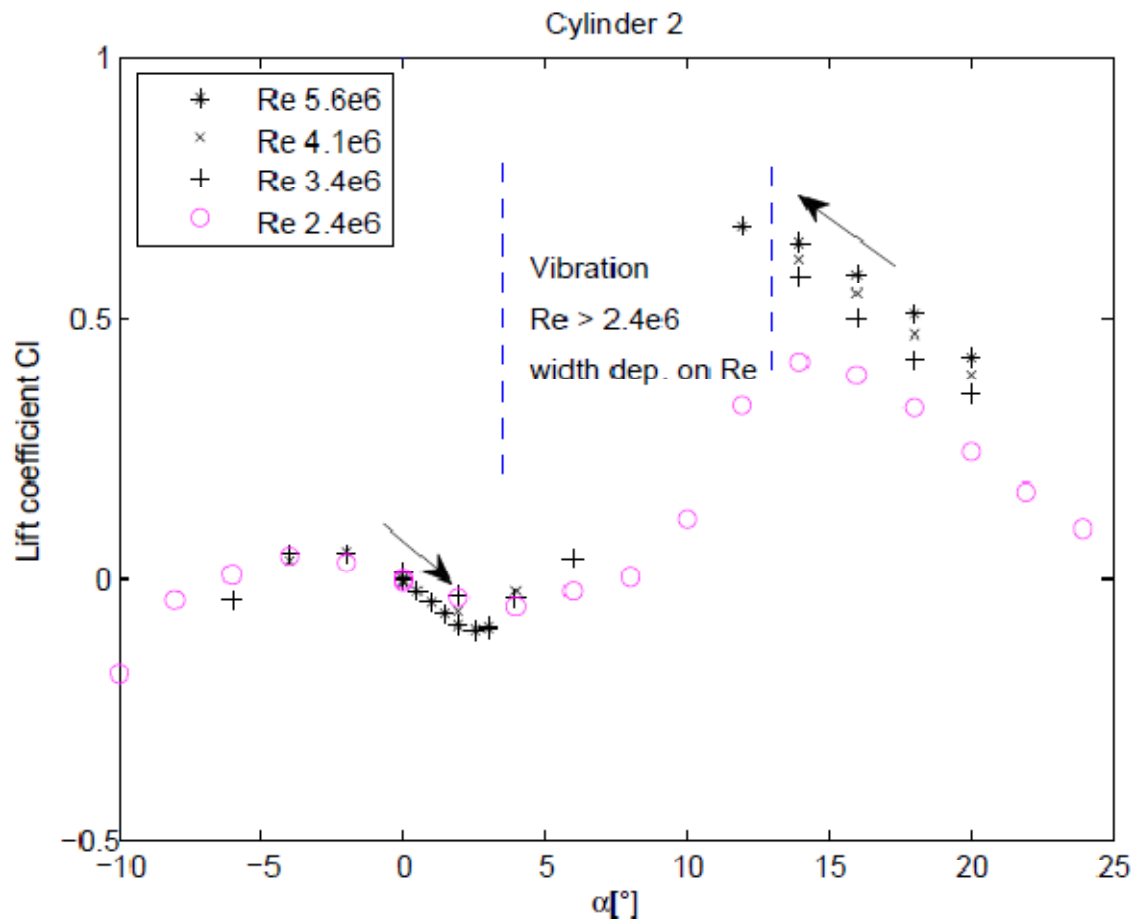


Figure 3.3 Lift coefficient of downwind cylinder as function on inflow angle  $\alpha$ .

Figure 3.3 shows the development of the mean lift coefficient  $C_L$  of the downwind cable element (Cyl<sub>2</sub>) as function of inflow angle and with Re as parameter. For the lowest  $Re \approx 2 \cdot 10^6$ ,  $C_L \approx 0$  in the inflow angle range  $-8 < \alpha < 8$  deg but increases steeply to  $C_L \approx 0.4$  at  $\alpha = 14$  deg. At higher Re measurements had to be abandoned in the inflow range  $4 < \alpha < 12$  deg due to very severe vibrations of the downwind cable element. These vibrations are judged to be caused by interference galloping as described in [2] and will be further treated in [3].

Figure 3.4 shows the development of the mean drag and lift coefficients  $C_D$ ,  $C_L$  of the upwind cable element (Cyl<sub>1</sub>) as function of inflow angle and with Re as parameter. For the highest Re achieved  $Re \approx 2.4 \cdot 10^6$ , a distinctive decrease of  $C_L$  is noted in the inflow range  $-6 < \alpha < 6$  deg. indicating a potential classical den Hartog galloping instability for the windward cable element.

		<b>Ponte sullo Stretto di Messina</b> <b>PROGETTO DEFINITIVO</b>		
Wind Tunnel Tests, Cables		Codice documento PB0035_F0.docx	Rev F0	Data 20/06/2011

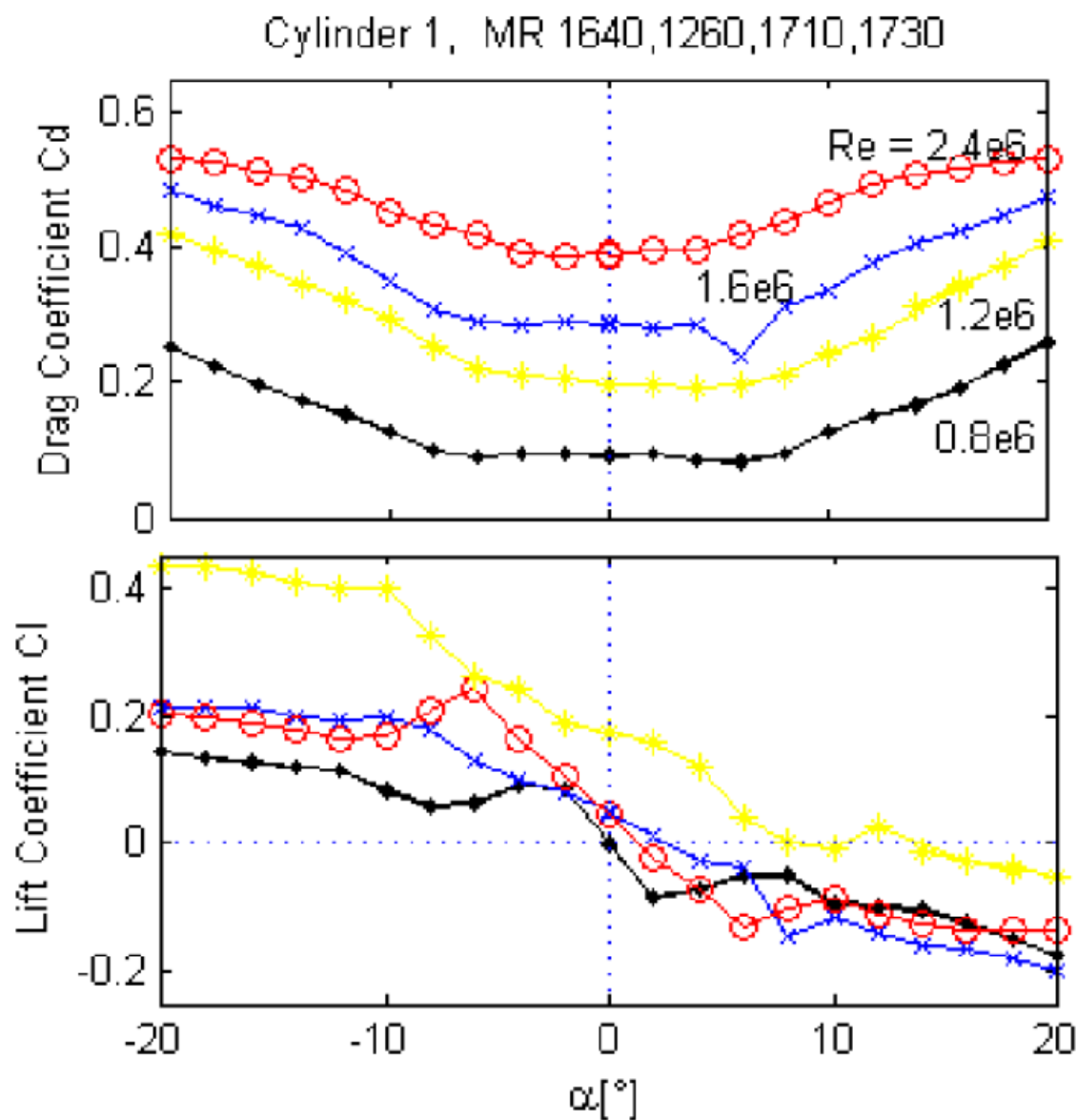




Figure 3.4 Drag and Lift coefficients for the upwind cylinder as function of inflow angle  $\alpha$ .

## 4 Conclusions

Measurements of lift and drag coefficients for a main cable model at full scale Reynolds' Numbers have provided wind load coefficients for the main cable and an indication of possible interference galloping and classical den Hartog galloping between the two cable elements.

		<b>Ponte sullo Stretto di Messina</b> PROGETTO DEFINITIVO		
Wind Tunnel Tests, Cables		Codice documento PB0035_F0.docx	Rev F0	Data 20/06/2011

A comparison of the lift and drag coefficients obtained from the present tests and available in the literature [4] is presented in Table 4.1 below.

*Table 4.1 Comparison of drag coefficients obtained from the present tests to values found in the literature.*

Drag coefficient $C_D$	ESDU 70013	Present sub-test C1, spacing 1.57·diameter	
	$Re < 3 \cdot 10^5$	$Re = 1.8 \cdot 10^5$	$Re = 5.6 \cdot 10^6$
Upwind element	$\approx 1.1$	1.0	0.5
Downwind element	$\approx -0.4$	-0.4	-0.1

Based on the results of sub-test C1 the following drag coefficients shall be applied for the twin main cable in design calculations:

Upwind cable element:  $C_D = 0.5$                       Downwind cable element  $C_D = -0.1$

Further evaluation of the potential galloping instabilities is presented in [3].

## 5 References

- 1 DNW-GUK report: Reynolds Number Effects in Flow around a Tandem-Cylinder from  $Re = 10^5$  up to  $6 \cdot 10^6$ . G. Schewe and M. Jacobs, 21.12.2010
- 2 Rusheweyh, H.: Dynamische Windwirkung an Bauwerken 2. Bauverlag 1982
- 3 EUROLINK S.C.p.A. CG1000-P-CL-D-P-SB-S3-00-00-00-04, Rev. B/ 2011-03-07, Aerodynamic calculations, cables. 2011.
- 4 ESDU data item 70013. Fluid Forces on Circular Cylinders for Application in General Engineering. Part I, Long Cylinders in Two-dimensional Flow. 1971.

		<b>Ponte sullo Stretto di Messina</b> <b>PROGETTO DEFINITIVO</b>		
Wind Tunnel Tests, Cables		<i>Codice documento</i> PB0035_F0.docx	<i>Rev</i> F0	<i>Data</i> 20/06/2011

## Appendix - Scope of Work

**Memo**

**Title** Eurolink s.c.p.a.  
Wind tunnel tests cables, Sub-tests C1, Scope of work

**Date** 7 July 2010

**To** Eurolink, EYA

**Copy** ALN

**From** SAMI

**COWI A/S**

Parallelvej 2  
DK-2800 Kongens Lyngby  
Denmark

Tel +45 45 97 22 11  
Fax +45 45 97 22 12  
www.cowi.com

## 1 Introduction

This memo details the scope of work for section model tests of the main cables, sub-test C1, following the overall aerodynamic design methodology for the Progetto Definitivo phase.

The objective of this test is to identify the risk of galloping oscillations of the main cable twin assembly. Experience from suspension bridges has shown that long unsupported stretches of cable bundles may enter into galloping instabilities at high wind speeds. For the Messina Bridge, the main cables are largely unsupported in the back stays with only a few hangers close to the pylons, and during construction before the deck is suspended.

## 2 Sub-test C1

Circular cross sections are known to be highly susceptible to Reynolds Number effects. It is therefore very important that the tests shall reflect the prototype Reynolds number range (up to  $6 \cdot 10^6$ , corresponding to a full scale wind speed of 75 m/s).

This can be achieved in the pressurised wind tunnel at DLR-Institut für Aeroelastik in Göttingen, Germany. With a maximum flow speed in the wind tunnel of 35 m/s and assuming a pressure of 70 bar, a main cable model diameter of 35 mm - 40 mm corresponds to Reynolds Numbers of approximately  $6.0 \cdot 10^6$  -  $6.5 \cdot 10^6$ . Forces are measured in a static set-up using a piezo-electric multi-component balance.

A preliminary test using only one main cable model shall be carried out to identify the lower end of the test Reynolds Number range, defined such that the critical region where the aerodynamic forces displays a sudden drop is included.

A model representing the twin cable assembly is then tested in the same Reynolds Number range.

The measurements shall establish the force coefficients in the along wind and cross wind direction  $C_x$ ,  $C_y$  for the down wind cable model as function of the

angle  $\beta$  between the wind direction and the line connecting the two cable model centres.

It is envisaged that  $\beta$  is varied in the range  $-4^\circ$  to  $20^\circ$  with at  $2^\circ$  increments which may be effectuated by moving the upwind cylinder in a vertical plane. The tests are envisaged to be repeated at approximately 10 Reynolds Numbers over the test range.

The tests shall be carried out in smooth flow,  $I_U < 2\%$ .

### **3 Model**

Preliminary contact Schewe/Larsen has indicated that DLR may be in possession of wind tunnel models which may be made available for the tests.

The surface of the main cables shall be slightly rough, corresponding to a wrapped and painted cable surface.

### **4 Data analysis and reporting**

The results of test runs shall be documented in a data report, which shall also documents the particulars of the section model.

The results of the analyses shall be reported with a complete documentation of the applied procedures and observations made in course of the tests.

Test data shall be provided in digital form upon request.

### **5 Time schedule**

It is envisaged that the tests can be completed and reported by mid September 2010.

IB 232 – 2011 C 01

G. Schewe, M. Jacobs

**Reynolds-Number Effects in Flow around a  
Tandem-Cylinder  
from  $Re = 10^5$  up to  $6 \cdot 10^6$**

Date: Jan. 2011  
Contractors: EUROLINK K.S.C.p.A. Milano  
Cost centre: 3004526  
Cost unit: 23215

This report contains:  
16 pages including  
12 figures  
1 table  
5 references

Duplication and distribution of this document as a whole or in excerpts as well as transmission of its contents to third parties is allowed only with the permission of  
(X) Client, (X) DLR

**German Aerospace Center (DLR)  
Institut für Aeroelastik  
Göttingen**

# Reynolds Number-Effects in Flow around a Tandem-Cylinder from $Re = 10^5$ up to $6 \cdot 10^6$

## Abstract

Force measurements on two circular cylinders in cross flow were performed for Reynolds numbers from sub- up to transcritical values. The tandem cylinder represented a twin cable assembly of the main cable of the Messina Bridge. The measurements were carried out in a special high Reynolds number facility, the DNW High Pressure Wind tunnel in Göttingen. The steady forces on each of both cylinders were measured using a both sided strain gauge balance. The Reynolds number was varied in the range from  $Re = 2 \cdot 10^5$  up to  $6 \cdot 10^6$ , the latter at a maximal pressure of  $p = 80$  bar and a maximal wind speed of  $U_{\max} = 38$  m/s. In all relevant Reynolds number ranges, for both cylinders polar diagrams were taken i.e. the dependence of the force coefficient upon the angle of incidence  $\alpha$ . At the maximal  $\alpha$  the blockage did not exceed 10%. As given by the prototype value, the dimensionless roughness of both cylinders was  $10^{-4}$  and the distance between the centres of the cylinders had a value of 1.56 times the diameter. For the purpose of comparison also the single cylinder was tested. For all configurations drastic changes of the global values depending on the Reynolds number were observed.

This report contains  
16 pages including  
14 figures  
1 table  
5 references

**German Aerospace Center (DLR)  
Institut für Aeroelastik  
Göttingen**

Head of Institute

Heads of Departments

Authors

Prof. Dr.-Ing. L. Tichy

Dr.-Ing. H. Hennings

Dr. rer. nat. G. Schewe  
Senior scientist

Dr.-Ing. M. Jacobs  
DNW Head of Project  
Management



## Introduction

The tests concern force measurement on two circular cylinders in cross flow, representing a twin cable assembly of the main cable of the Messina Bridge. The reason for the tests are to look for the risk of flow induced vibrations at the prototype of the bridge.

Ruscheweyh (1983) described the aeroelastic interference effects for a tandem cylinder arrangement at subcritical Reynolds numbers ( $Re \approx 10^5$ ) as follows: Selfexcited oscillation of the downwind cylinder can occur for small distance  $d/D < 3$  and when a critical angle of incidence is exceeded. Below the critical value the downstream cylinder is completely in the wake of the first one and consequently there is no lift or traverse force. Beyond the critical angle the flow is able to stream with high velocity through the gap between the two cylinders producing high negative pressure associated with high lift force on the downwind cylinder. The lift forces i.e. the across wind forces have the tendency to center the downstream cylinder, that is, draw it toward the centreline of the wake, as it is formulated in Simiu & Scanlan (1986). In the polar diagram  $Cl(\alpha)$  this behaviour is reflected in a steep increase of the lift with positive slope beginning at the critical angle.

The main objective of the tests, is to find out, if this behaviour, representing aeroelastic stability and typical for subcritical Reynolds numbers is depending on the Reynolds number. The desired maximal Reynolds number is  $Re \approx 6 \cdot 10^6$  based on the prototype value of the cable diameter 1.28 m and an assumed maximal wind speed of  $U_{max} = 60$  m/s. The distance between the cables is 2m.

The measurements were performed in a special high Reynolds number facility, the DNW High Pressure Wind tunnel in Göttingen. This continuous running wind tunnel was especially designed for investigating civil engineering structures in incompressible flow and at very high Reynolds numbers up to  $Re \approx 10^7$ . Many investigations concerning Reynolds number effects in flow around bluff bodies have been performed in this facility, which are partly summarized in Schewe (2001). In particular results and interpretations about flow around single smooth cylinders can be found in Schewe (1983, 1986).

The steady forces on both cylinders were measured in individual test runs using a both sided strain gauge balance, which is mounted on a turn table. The force coefficients concern the along wind component drag  $C_d$  and the crosswind direction the lift  $C_l$ . The Reynolds No was varied in the range from  $Re = 2 \cdot 10^5$  up to  $6 \cdot 10^6$ , the latter at a maximal pressure of  $p = 80$  bar and a maximal wind speed of  $U_{max} = 38$  m/s. In all relevant Reynolds No ranges, for both cylinders polar diagrams were taken i.e. the dependence of the force coefficient upon the angle of incidence  $\alpha$  in the range  $-20^\circ < \alpha < 20^\circ$ . The diameter of the cylinders and with that the aspect ratio was chosen such that also at the maximal angle of incidence the blockage did not exceed 10%.

The surface roughness can play an important role regarding Reynolds number effects, thus some effort was necessary to achieve the desired dimensionless roughness given by the prototype value of  $10^{-4}$ .

The distance between the centres of the cylinders was rather close i.e. 1.56 times the diameter. Concerning the general test condition we can state that, the desired maximal Reynolds number was reached without compromising the size of the model, Mach number effects (0.1), blockage effects (6.3%), surface roughness or turbulence in the oncoming flow.

## Experimental Arrangement

### Wind tunnel

The high pressure wind tunnel shown in Figure 1 is built with the purpose of achieving very high Reynolds numbers in incompressible flow, thus making the tunnel ideal for wind engineering purposes. The entire wind tunnel tube, which is of the closed return type, can be pressurised up to 100 bar, which allows maximum Reynolds numbers of  $10^7$  to be achieved in incompressible flow. The main particulars of the wind tunnel are as follows:

- Maximum flow speed  $U = 38 \text{ m/s}$
- Size of square test section  $0.6 \times 0.6 \text{ m}^2$
- Pressure range  $1 \leq p \leq 100 \text{ bar}$
- Reynolds number range  $10^4 < Re < 10^7$  based on dimension  $l = 0.06 \text{ m}$
- Contraction ratio 5.6:1
- Power consumption  $N = 470 \text{ kW}$

The closed test section is 1 m long and can be removed from the wind tunnel by means of an air lock system while the tunnel tube is kept under pressure. The turbulence intensity of the flow in the test section increases slightly with increasing  $Re$  but is less than 0.4%.

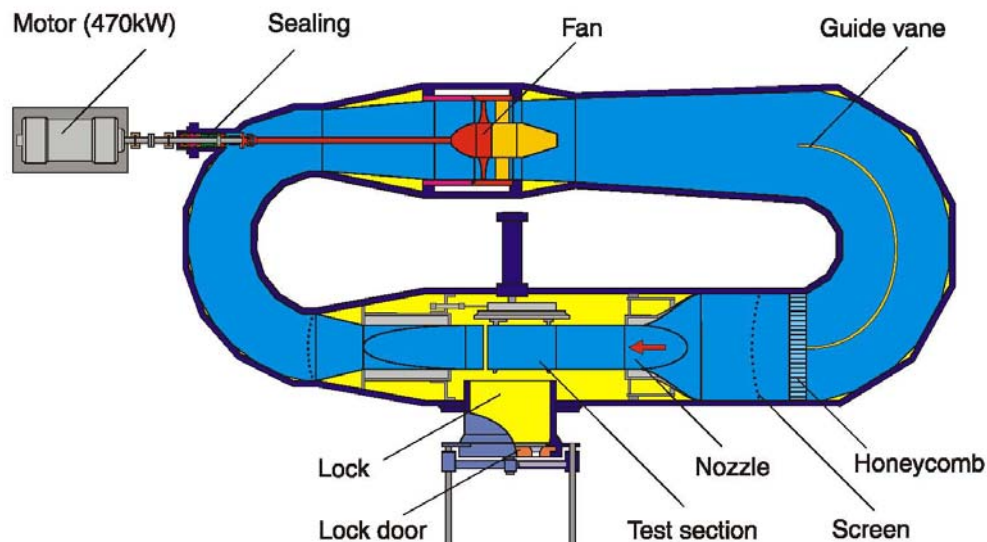


Figure 1 High pressure wind tunnel of German-Dutch Wind Tunnels (DNW) in Göttingen, Germany.

In the high pressure wind tunnel it is in principle possible to investigate the same model at Reynolds numbers spanning 3 orders of magnitude by merely varying the flow parameters.

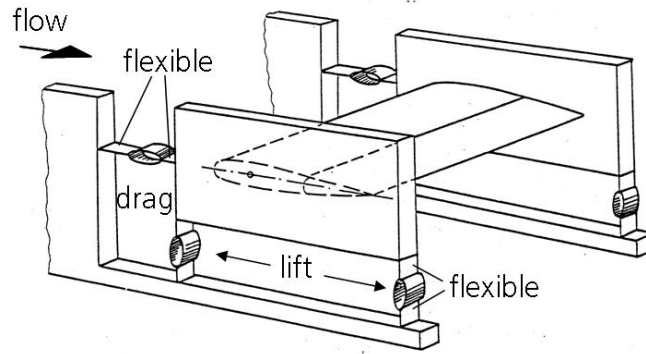


Fig. 2: Principal sketch of a strain gauge balance for 3-component force measurements. The strain gauges are affixed on the individual rings

### Strain gauge balance

Fig. 2 depicts the principle of a typical strain gauge balance for three component measurements on a two-dimensional airfoil-model. The model is fixed at both ends by a force conducting plate supported by three elastic ring elements. The ring elements, on which the strain gauges are applied, represent the force transducers. The flexible parts are necessary for the following reason: When considering for example the drag direction (x), it is obvious that a sufficient measuring deflection in the ring element for drag requires a corresponding flexibility of the lift measuring elements also in the x-direction and vice versa. In other words, the necessary measuring deflections for every component require a mechanical decoupling of the individual components, which are perpendicular to the desired one. In reality, the strain gauge balance of the High pressure wind tunnel is more sophisticated using six high end force transducers manufactured by Hottinger and special elastic elements for decoupling. The balance was oriented in such away that the main drag force was acting on the four elements, that is also the reason that the lowest eigenfrequency in drag direction is higher than in lift direction (figure 5a).

### Test Setup

The leading cylinder will be attached in such away that the angle  $\alpha$  between the wind direction and the line connecting the two cylinder centres can be varied by the turn table (figure 3 and 4). The cylinder diameter is  $d = 0.038\text{m}$ , thus for the maximal angle desired  $\alpha = 20^\circ$  the blockage is not higher than about 10%. The distance  $D$  between the cylinders is  $D/d = 1.56$ .

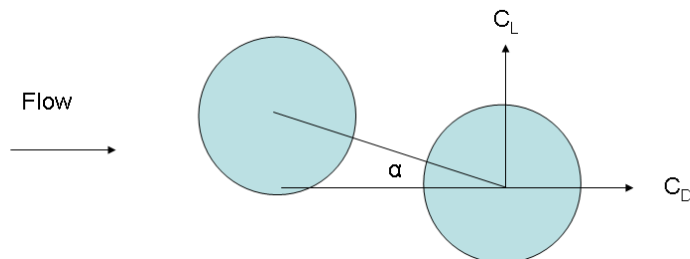


Figure 3: Coordinate system of cylinder arrangement. The cylinder under force-measurement remains always in the center of the turn table. Thus the second cylinder is moved around the central one.

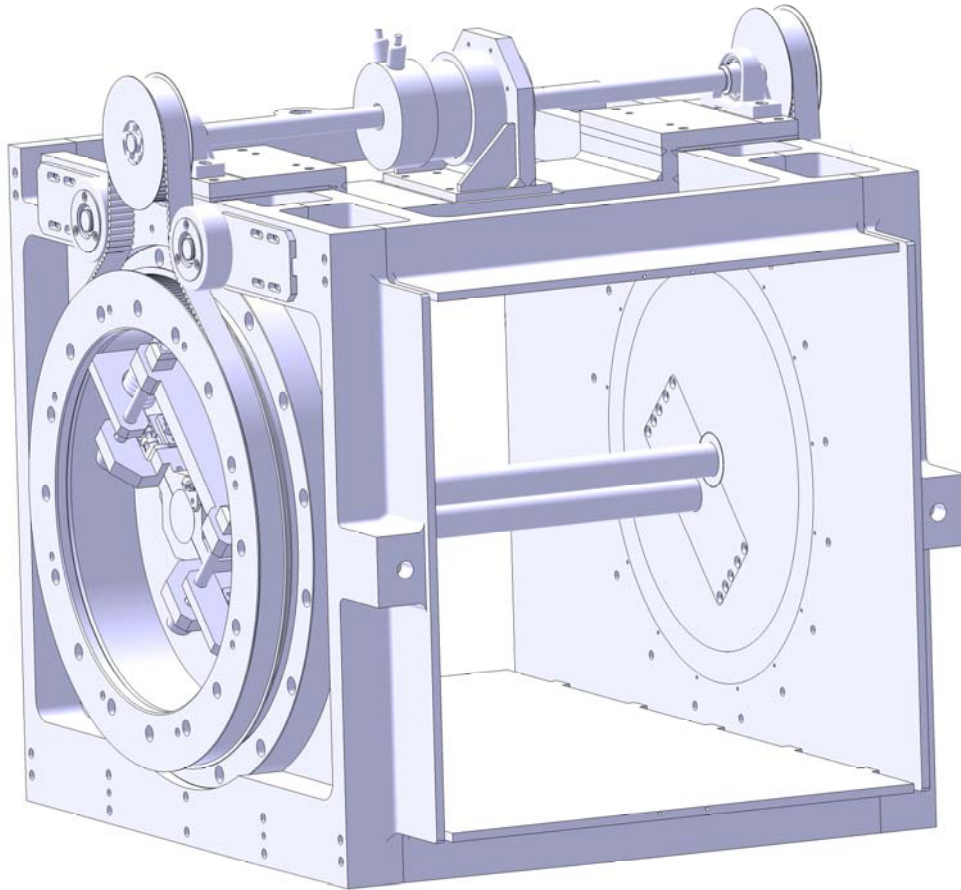


Figure 4: Test section of the DNW-High Pressure Wind Tunnel including the tandem cylinder.

The drag- and lift forces on the cylinder in the center will be measured by a strain gauge balance. The second cylinder is mounted at the wind tunnel wall and can be rotated by the turn table (see photos). The force coefficients are presented in the fixed wind tunnel system.

### Double Cable Model and structural Properties

The cylinders, manufactured from aluminium, were milled and then grinded down to the desired surface roughness of  $k = 5 \mu\text{m}$  corresponding  $k/d = 10^{-4}$ .

The lowest eigenfrequencies of the system balance-model (RBM) are  $f_z = 87.3 \text{ Hz}$  in lift- and  $f_x = 128.4 \text{ Hz}$  (slightly increasing with pressure) in drag direction. The corresponding damping values (relative to critical) are  $\delta z = 0.35\%$  and  $\delta x = 0.37\%$ . The weight of the moving mass inside the balance was determined by inverting the balance and has a value of 14 kg.

D: center-to-center spacing

d: diameter of the cylinder  $d = 0.038 \text{ m}$

$D/d = 1.56$

Surface roughness  $k = 5 \mu\text{m}$

$k/d = 10^{-4}$

Reynolds number related to d

Aspect ratio: 1: 15.8

Blockage: 6.3% for  $\alpha = 0^\circ$



Figure 5 a: Photo of the test section, the turn table and the balance. In the centre there is the clamped cylinder under test. The three force transducer can be recognized by its bellows.



Figure 5 b: The second cylinder is attached in holes of the walls by clamping collars.

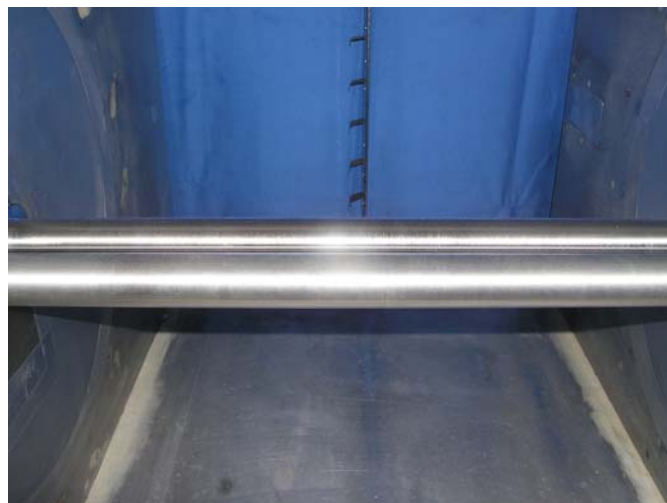


Figure 5 c: View inside the test section

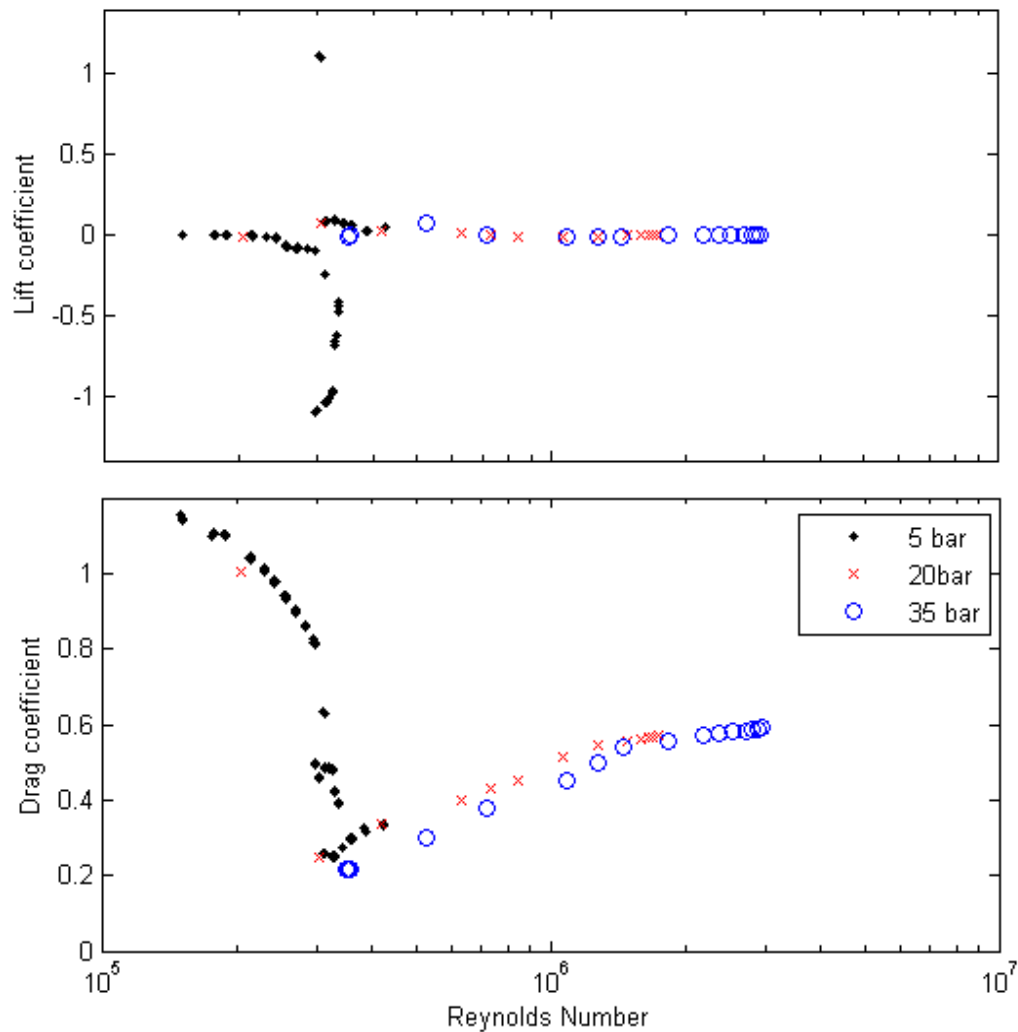


Figure 6: Drag and lift coefficient for a single cylinder depending on the Reynolds number (here roughness  $1e-3$ )

### Results: Single Cylinder

Figure 6 shows the drag and lift coefficient upon the Re No for a single cylinder. Other than for the following tandem arrangement the roughness related to the diameter was  $k/d = 10^{-3}$ , the value which was desired in a first stage of the project.

If one compares the shape of the curve with the corresponding one for a smooth circular cylinder (Schewe 1983), then it is obvious that there is no extended supercritical range with low and constant drag coefficient. But the location of the critical Re No regime at  $3 \times 10^5$  is nearly the same. Also the occurrence of steady asymmetric states, with both signs (nota bene!) could be observed, although the relative high surface roughness is nearly two orders of magnitude higher. The long transition regime begins after the drag crisis, the plateau of the transcritical range is reached at about at  $Re \approx 3 - 4 \times 10^6$ , also similar as in the case of the smooth cylinder.

It should be remarked that the differences in the transition region  $3.5e5 < Re < 1e6$  is not caused by less measurement accuracy. Here the flow is very sensitive to even the smallest variations in the surface properties. In order to simulate the first version of the cable surface



structure, the model has a desired fine structure with very fine helical rills (grooves). Before the measurement at 35bar the model was cleaned. Probably the cleaning process filled up a little bit the rills, reducing the surface roughness. The consequence could be a small reduction of the drag coefficient. This effect becomes less significant when approaching transcritical Reynolds numbers.

### Results: Tandem Cylinder

In figure 7 are plotted the drag coefficients for both individual cylinders depending on the Reynolds number at  $\alpha = 0^\circ$ . The appearance of the curve for the front cylinder (Cyl<sub>1</sub>) is similar to the behaviour of a single smooth circular cylinder (Schewe 1983), thus we can use the same nomenclature concerning sub-, super- and transcritical Reynolds numbers. In particular the location of the critical Reynolds number regime at  $3 \cdot 10^5$  is nearly the same. There is also a long supercritical range up to about  $Re \approx 10^6$ . After a second rather long transition regime, the plateau of the transcritical range is reached at about at  $Re = 5 \cdot 10^6$ . At the latest here one has to take into account that more or less regular vortex shedding may reappear.

The curve of the second cylinder is the inverse of the first one.

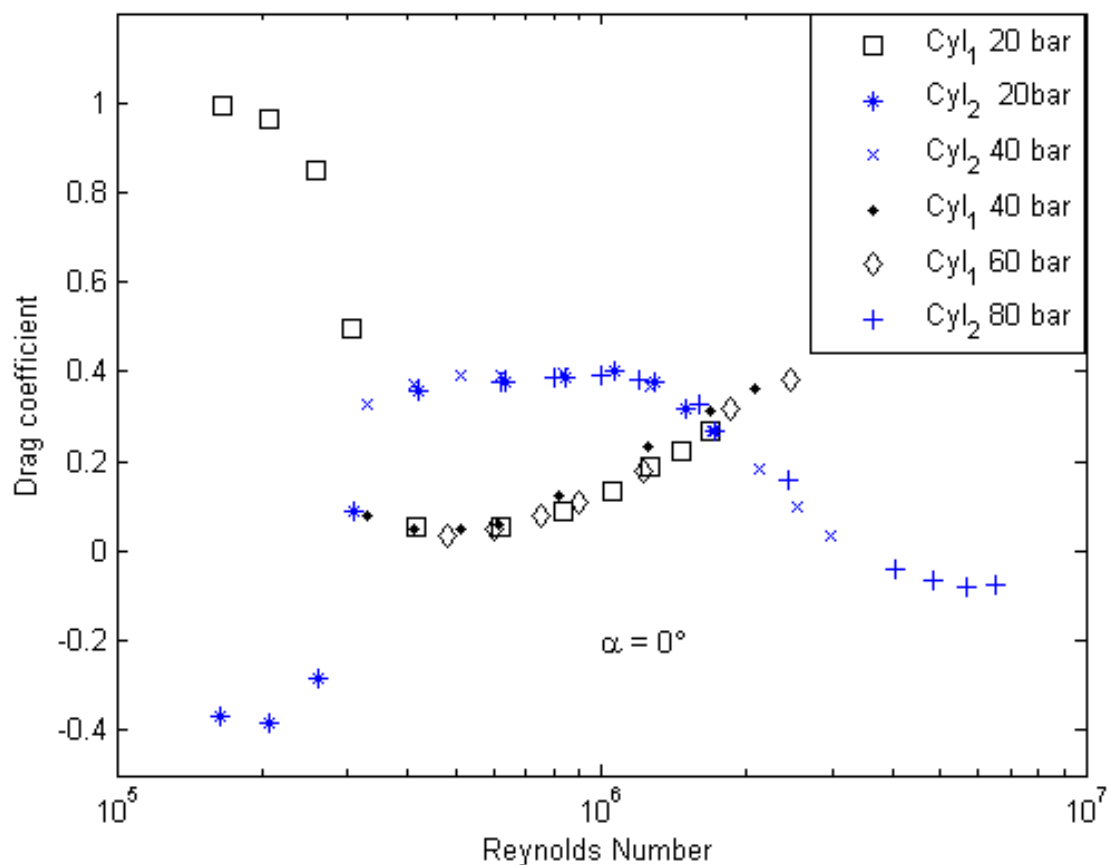


Figure 7: Drag coefficients for both individual cylinders upon the Reynolds number at  $\alpha = 0^\circ$

Concerning the tests on the first cylinder we were not able to take measurement for  $Re > 2.4e6$ . For  $\alpha = 0^\circ$  and  $p = 80$  bar the violent vibrations in lift direction ( 87Hz ) began at a wind speed of about 14m/s ( $N = 300$ rpm) i.e. at nearly the same  $Re$  No at which we already had measured (60bar). With  $\alpha = 20^\circ$  we tried to cross the vibration range (flow speed sweep) but even at about 28 m/s ( $N = 600$ ) the violent vibration did not cease, thus we had to break off.

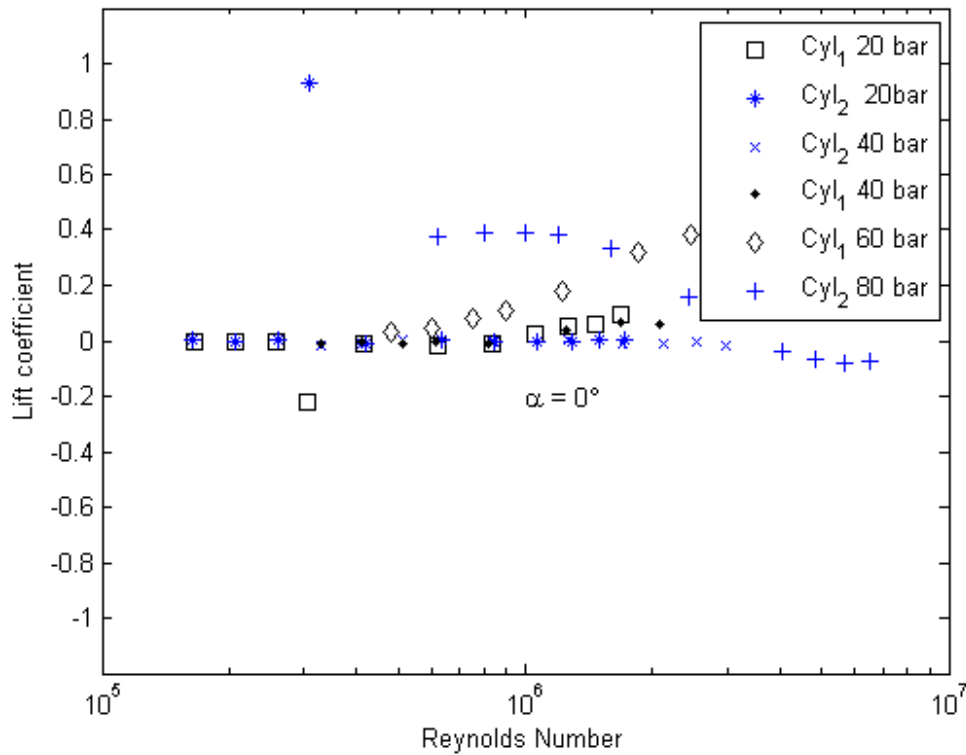


Figure 8: Lift coefficients for both individual cylinders depending on the Reynolds number at  $\alpha = 0^\circ$ .

Figure 8 displays the corresponding steady lift coefficients for both individual cylinders depending on the Reynolds number at  $\alpha = 0^\circ$ . Also in case of the tandem cylinder, in the transition regimes, there are steady asymmetric flow states as in case of a single cylinder. In the critical regime, for the downwind cylinder there is a steady lift force of  $Cl \approx 1$ . We can imagine that, if we had repeated the experiment several times, then also the other sign would have been occurred. The asymmetric states are caused by one sided separation bubbles and can be interpreted as bifurcation phenomena. Thus, under optimal symmetrical test conditions and  $\alpha = 0^\circ$ , the side where the bubble is formed first, is unpredictable (Schewe 1986).



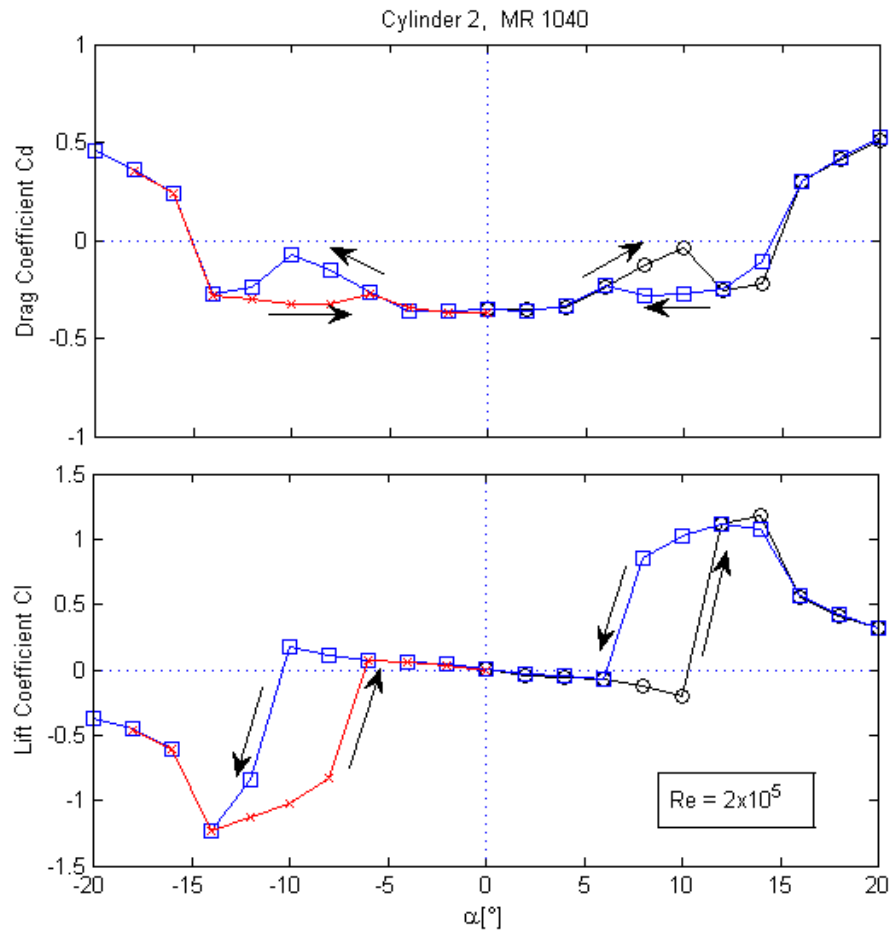


Figure 9: Polar diagram for drag- and lift coefficient on the **second cylinder** for the subcritical Reynolds number-case.

In figure 9: the polar diagram for drag- and lift coefficient on the second cylinder for the subcritical Re No-case is shown. The arrows indicate the direction of the angle variation, thus the strong hysteresis effects are obvious. The sudden increase of the lift, here at  $\pm 10^\circ$ , is responsible for the propensity to selfexcited oscillations of the downwind cylinder. The acrosswind forces have the tendency to centre the downstream cylinder. The point symmetry of the curves reflects the good test conditions, even in the case of relatively small forces at the smallest Reynolds number measured.

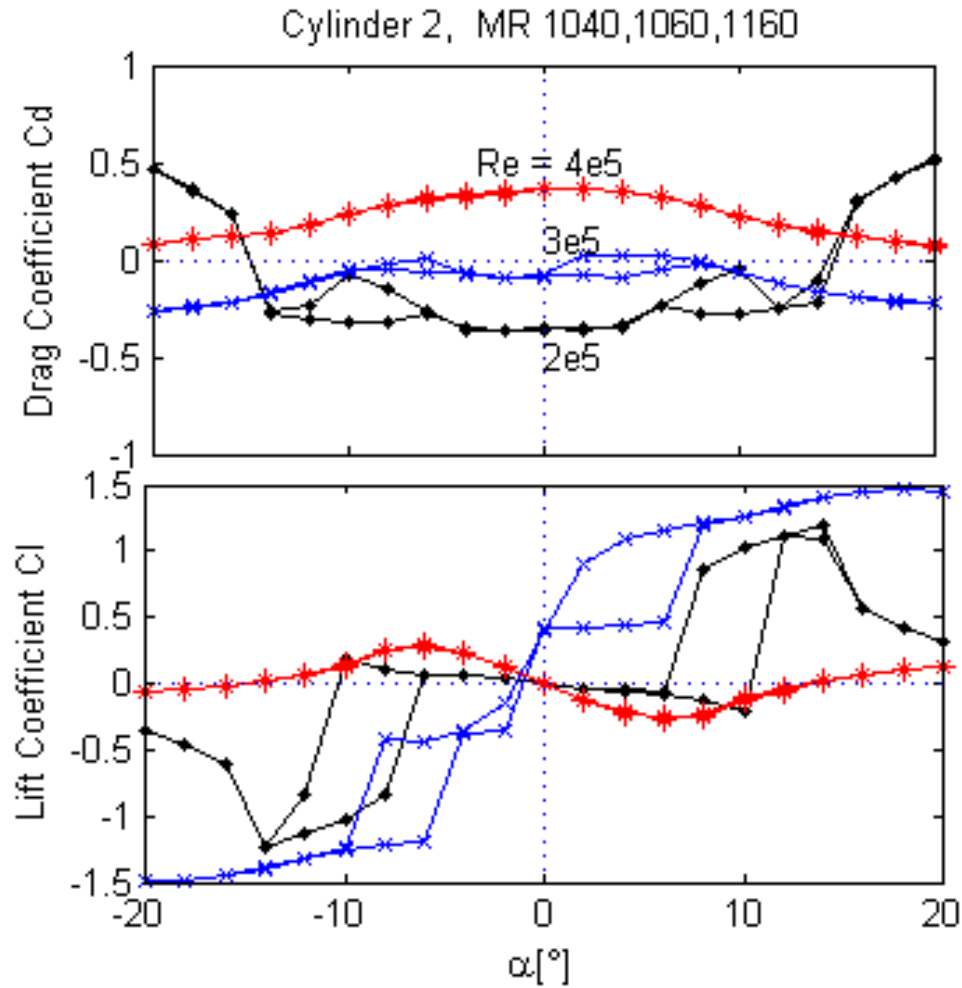


Figure 10: Polar diagram for the drag- and lift coefficient on the **second cylinder** in and near the critical Reynolds number range. The subcritical case corresponds to figure 9.

The transition from sub- to supercritical Reynolds numbers reflected in the polar diagram for the drag- and lift coefficient on the second cylinder is illustrated in figure 10. The most obvious change to supercritical Re is the fact, that there is no longer the sudden increase in the lift. Concerning the drag coefficient the sign changes not only for  $\alpha = 0^\circ$  but also for a larger range of angles around. For  $Re = 3e5$  and  $\alpha = 0^\circ$  there is steady lift.

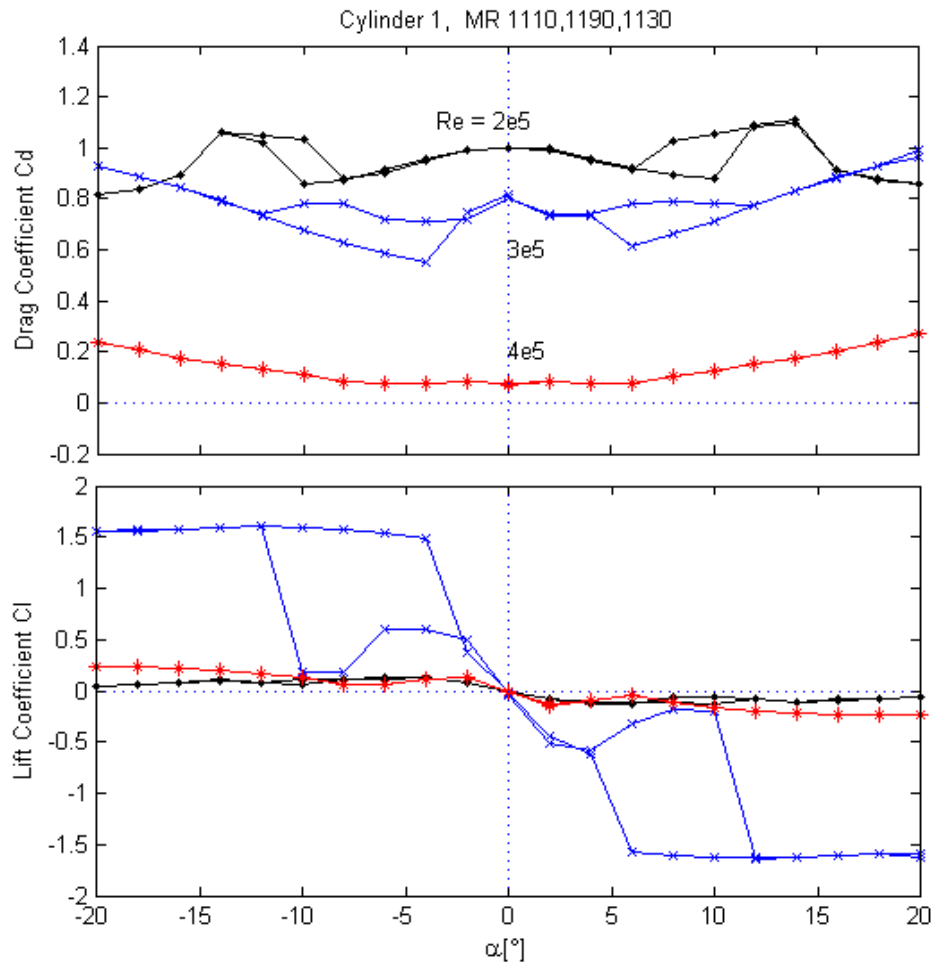


Figure 11: Polar diagram for the drag- and lift coefficient on the **first cylinder** in and near the critical Reynolds number range.

Figure 11 displays the corresponding polar diagram for the drag- and lift coefficient on the first cylinder. In particular directly in the critical regime at  $Re = 3e5$  there are strong lift forces with increasing angle, which are coupled with hysteresis and the slopes for both cylinder positions are opposite each other.

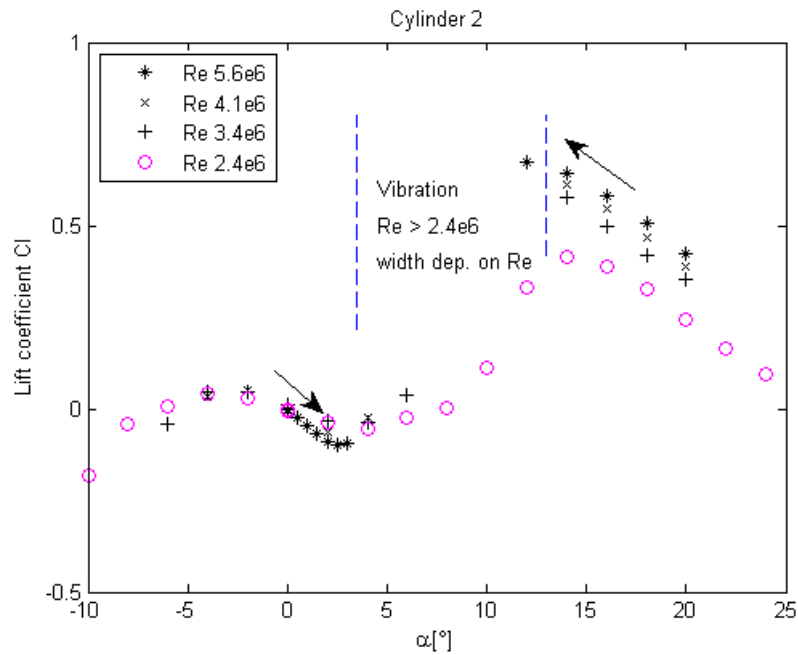


Figure 12: Polar diagram for lift coefficient on the second cylinder for the very high Reynolds number-case

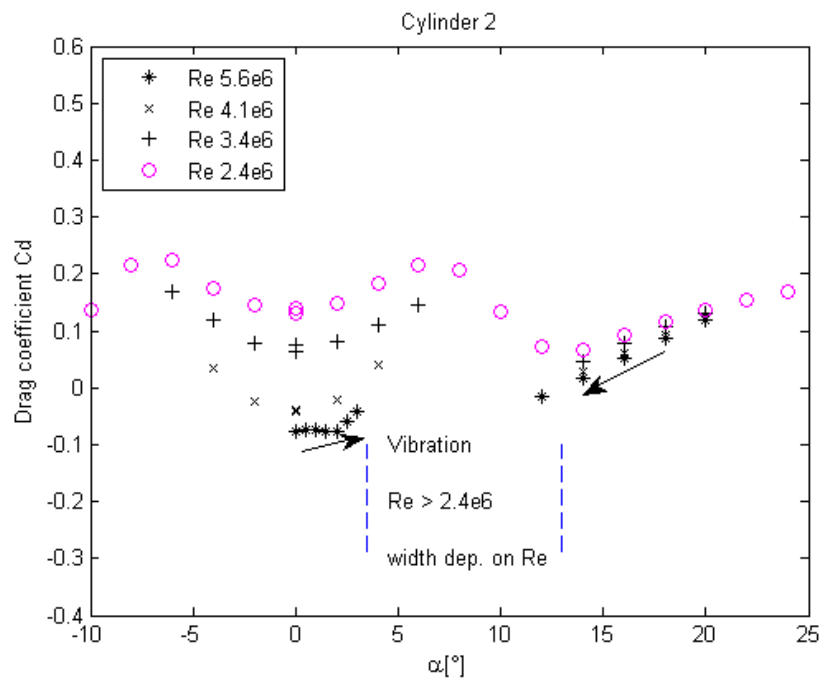


Figure 13: Polar diagram for the drag coefficient on the **second cylinder** for the very high Reynolds number-case

The figures 12 and 13 show the behaviour of the lift- and drag coefficient depending on  $\alpha$  for the Re No approaching the desired value of  $Re = 6 \cdot 10^6$  (in the transcritical range). At  $Re = 2.4e6$  there was the last possibility to take a full polar diagram for the entire range of  $\alpha$ . Beginning at  $Re = 3.4e6$ , there was a range of angles where violent vibrations in lift direction (87.3Hz) occurred. The arrows indicate how we approached the vibration range. Although we have no measurement in the unstable region, we can conclude from the rest of the curve that with increasing  $\alpha$  there must be a drastic increase in the lift force. This behaviour seems to be

similar as in the subcritical case displayed in the figure 9. The vibrations occurred also at corresponding negative angles, but in order to preserve the test setup, we decided to take no corresponding measuring point. Obviously there was a risk for damage.

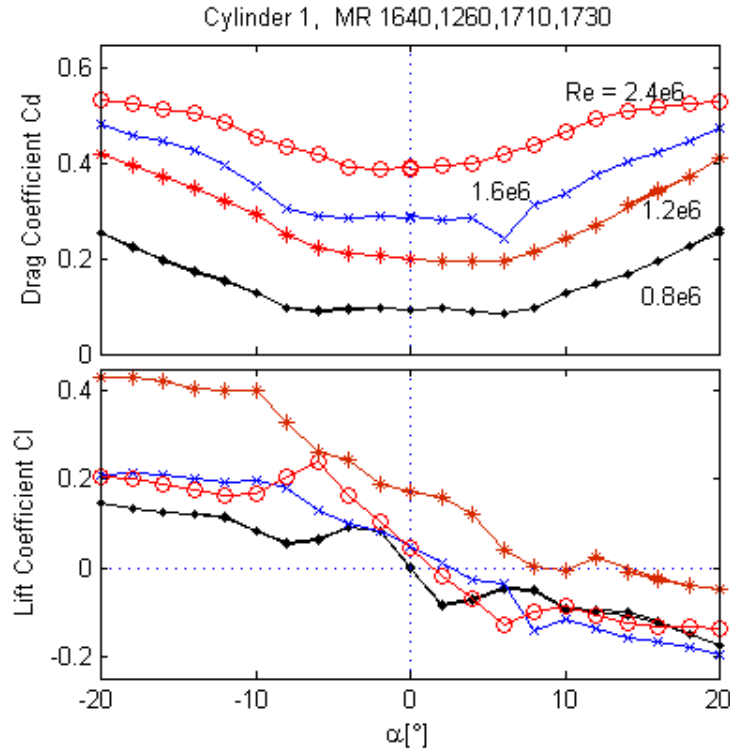


Figure 14: Polar diagram for the drag- and lift coefficient on the **first cylinder** for the Reynolds number approaching the transcritical range.

In figure 14 we see the polar diagram for the drag- and lift coefficient concerning the **first cylinder**, when the Reynolds number is approaching the transcritical range. For  $Re = 1.2e6$  there is still a steady asymmetry in the lift.

As mentioned in the context of figure 7, we were not able to take measurement for  $Re > 2.4e6$ . For  $\alpha = 0^\circ$  and  $p = 80$  bar the violent vibrations in lift direction ( 87Hz ) began at a wind speed of about 14m/s i.e. at nearly the same  $Re$  No at which we already had measured (60bar). We had the impression that in particular around  $\alpha = 0^\circ$  the situation was prone to vibrations, thus with  $\alpha = 20^\circ$  we tried to cross the vibration range (flow speed sweep) but even at about 28 m/s, the violent vibration did not cease and we had to break off. It seemed that vortex resonance phenomena as well as selfexcited oscillation could have been the reason for the vibrations. Selfexcited oscillations could be associated with the negative slope in the characteristic of the lift, which (the slope) increases with increasing  $Re$ . At the highest  $Re$  measured for this case,  $Re = 2.4e6$ , the lift is nearly linear in the range  $\alpha = \pm 6^\circ$  with negative slope.

The derivative of the lift for this case is  $\partial Cl / \partial \alpha = -1.7$ . Applying the den Hartog criterion yields:

$$\partial Cl / \partial \alpha + C_d = -1.7 + 0.4 < 0 \text{ indicating instability.}$$

Unfortunately it is very difficult to obtain the vortex shedding frequency, when using strain gauge balances. By appropriate small variations of the flow speed, we tried to find a significant (Strouhal) peak, but so close to the eigenfrequency of the force measuring system, in the unsteady signal of the balance, we could not find an indication for a spectral Strouhal peak.

## References

- Ruscheweyh, H. 1983 Aeroelastic interferences effects between slender structures.  
J. Wind Eng. and Ind. Aerodynamics, 14 p 129-140
- Schewe, G. 1983 On the force fluctuations acting on a circular cylinder in crossflow  
from subcritical to transcritical Reynolds numbers. J. Fluid Mech. 133, p. 265
- Schewe, G. 1986 Sensitivity of transition phenomena to small perturbations in flow  
round a circular cylinder. J. Fluid Mech. 172, p. 33
- Schewe, G. 2001 Reynolds-number effects in flow around more-or-less bluff bodies.  
J. Wind Eng. Ind. Aerodyn. 89, p. 1267
- Simiu, E., Scanlan, R. H. 1996 Wind Effects on Structures. John Wiley & Sons  
3. Ed, p. 240

## 1.1 List of all Tests

Polar Number	Name of Run	Name of Polar	Number of Points
<b>Single Cylinder Roughness 30 um</b>			
310	Pk=5bar	U=10-32m/s_kalibriert	107
360	Pk=20bar	U=10-32m/s	13
440	Pk=35bar	U=10-32m/s_kalibriert	16
1040	Pk=5bar	Re=0.2_Mio	51
1060	Pk=5bar	Re=0.4_Mio	51
1160	Pk=5bar	Re=0.3_Mio	51
1330	Pk=20bar	Re=0.4_Mio	51
1350	Pk=20bar	Re=0.8_Mio	28
1370	Pk=20bar	Re_0.4-1.6_alpha0	9
1390	Pk=20bar	Re=1.2_Mio	28
1410	Pk=20bar	Re=1.6_Mio	28
1430	Pk=20bar	Re_0.4-1.6_alpha0	11
1510	Pk=40bar	Re_0.5-3.2_alpha0	10
1530	Pk=40bar	Re_0.5-3.2_alpha2	10
1550	Pk=40bar	Re=0.8_Mio	51
1570	Pk=40bar	Re=1.6_Mio	27
1590	Pk=40bar	Re=2.4_Mio	27
1780	Pk=60bar	Re_1.0-4.4_alpha0	11
1800	Pk=60bar	Re=1.6Mio	27
1820	Pk=60bar	Re=3.2_Mio	7
1840	Pk=60bar	Re=3.2_Mio	5
1860	Pk=60bar	Re=3.2_Mio	5
1880	Pk=60bar	Re=4.0_Mio	4
1900	Pk=60bar	Re=4.0_Mio	3
1920	Pk=60bar	Re=4.0_Mio	5
1950	Pk=80bar	Re_0.8-6_alpha0	10
1970	Pk=80bar	Re=5.68_Mio	8
1990	Pk=80bar	Re=5.68_Mio	6
2020	Pk=5bar	StatischeReihe-110_-60	51
2050	Pk=5bar_vl	StatischeReihe70_120	51
1090	Pk=5bar_vl	StatischeReihe70_120	51
1110	Pk=5bar_vl	Re=0.2_Mio	51
1130	Pk=5bar_vl	Re=0.4_Mio	51
1190	Pk=5bar_vl	Re=0.3_Mio	51
1220	Pk=20bar_vl	Re=0.4_Mio	51
1240	Pk=20bar_vl	Re=0.8_Mio	27
1260	Pk=20bar_vl	Re=1.2_Mio	30
1280	Pk=20bar_vl	Re=1.6_Mio	12
1300	Pk=20bar_vl	Re=1.6_Mio	27
1460	Pk=20bar_vl	Re_0.4-1.6_alpha0	11
1480	Pk=20bar_vl	Re=1.6_Mio	4
1620	Pk=40bar_vl	Re_0.5-3.2_alpha0	8
1640	Pk=40bar_vl	Re=0.8_Mio	51
1660	Pk=40bar_vl	Re=1.6_Mio	27
1690	Pk=60bar_vl	Re=1.6_Mio	11
1710	Pk=60bar_vl	Re=1.6_Mio	28
1730	Pk=60bar_vl	Re=2.4_Mio	27
1750	Pk=60bar_vl	Re_1.0-4.4_alpha0	7

## Appendix



## Polars

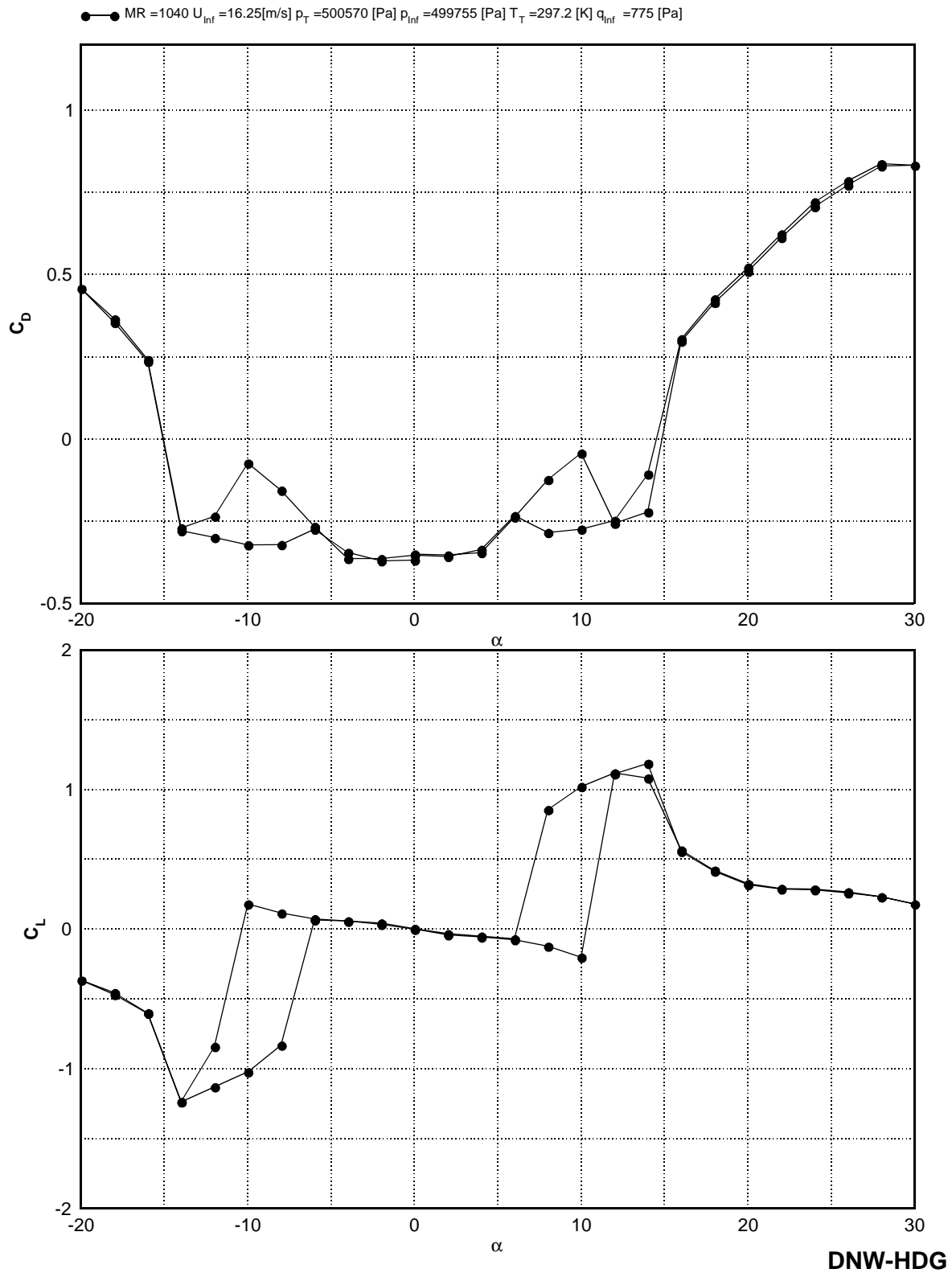


Figure 1 2'nd Cylinder  $Re = 0.199$  [Mio]  $Pk=5bar$

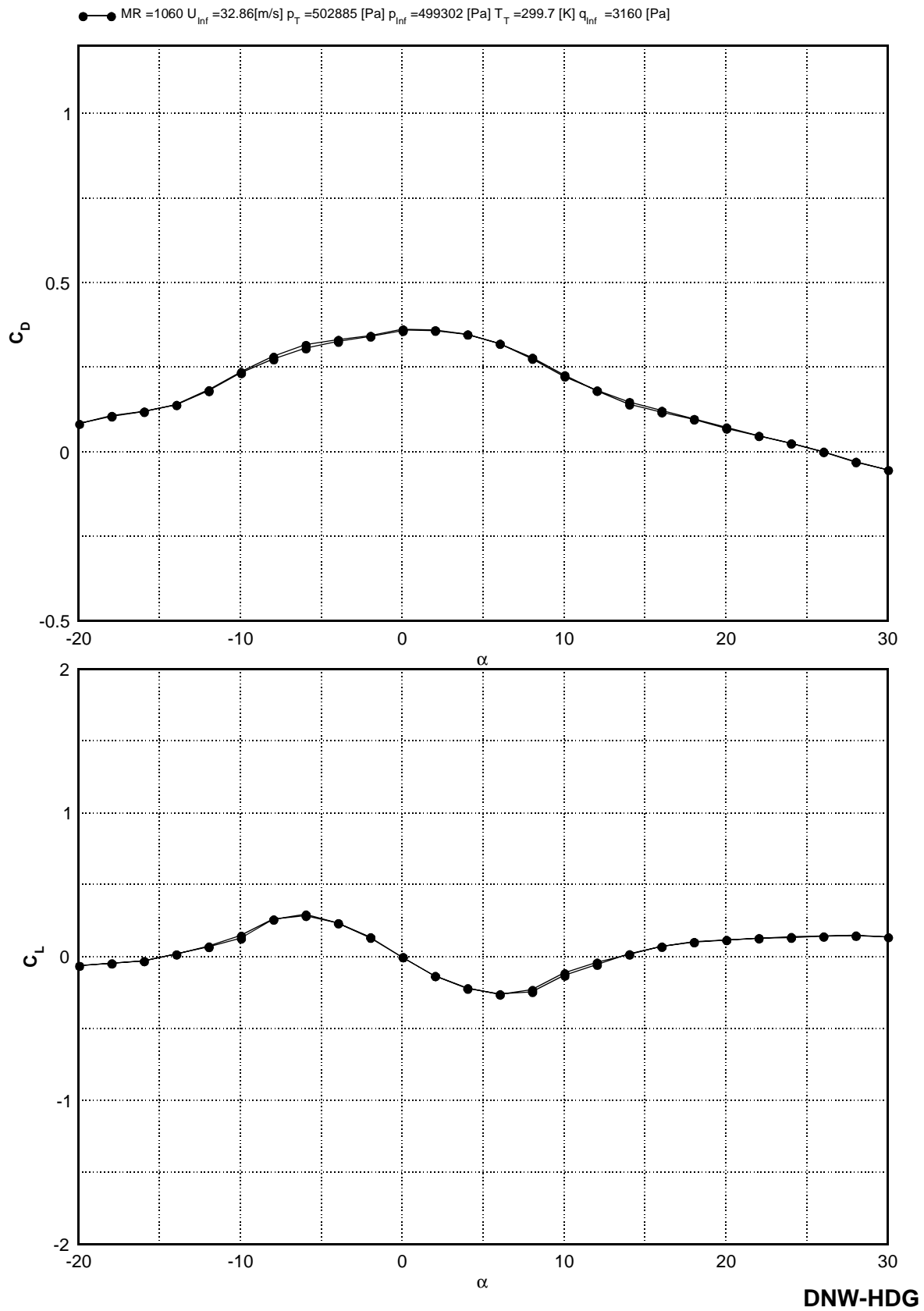


Figure 2 2'nd Cylinder  $Re = 0.399$  [Mio]  $P_k = 5\text{bar}$

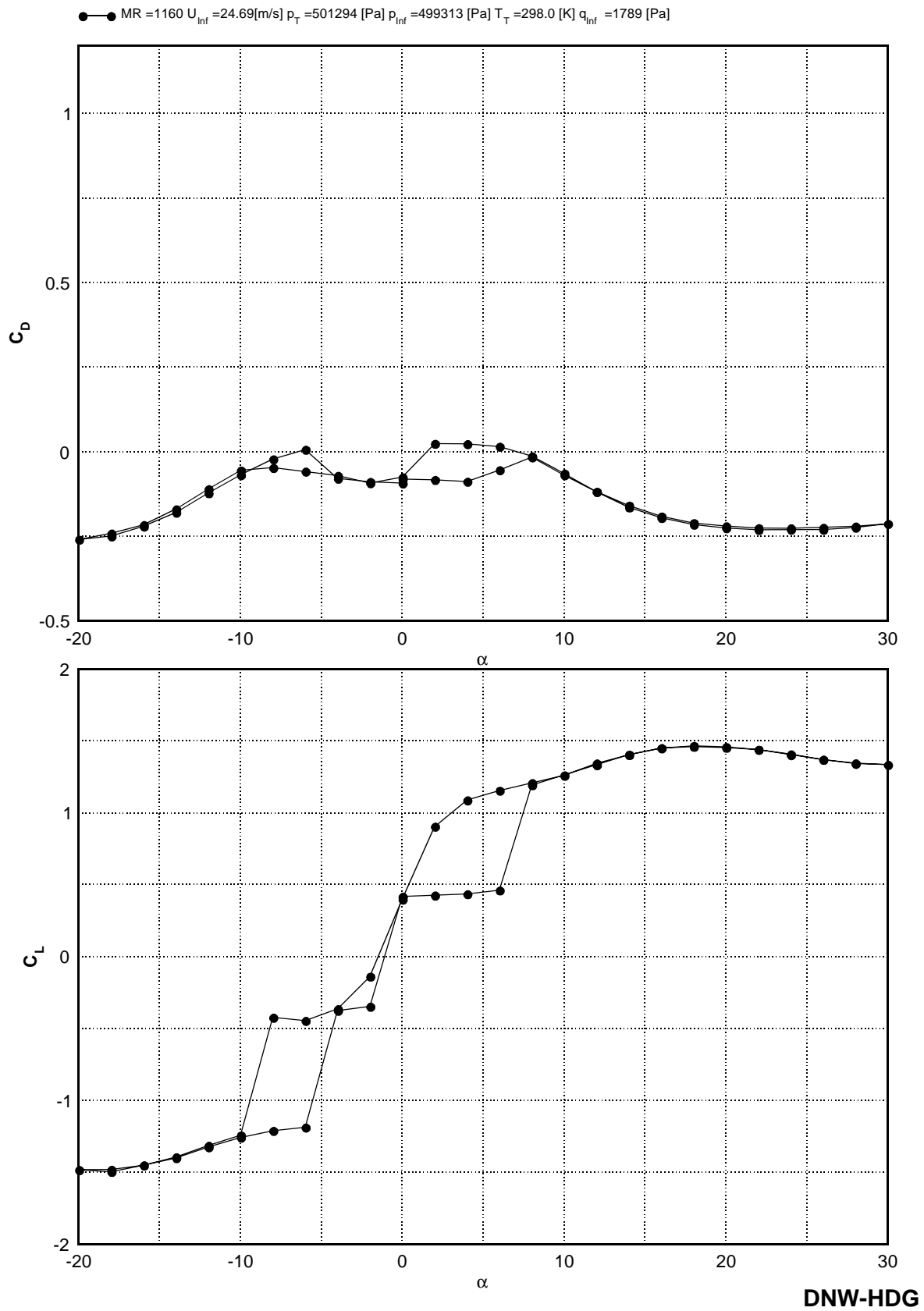
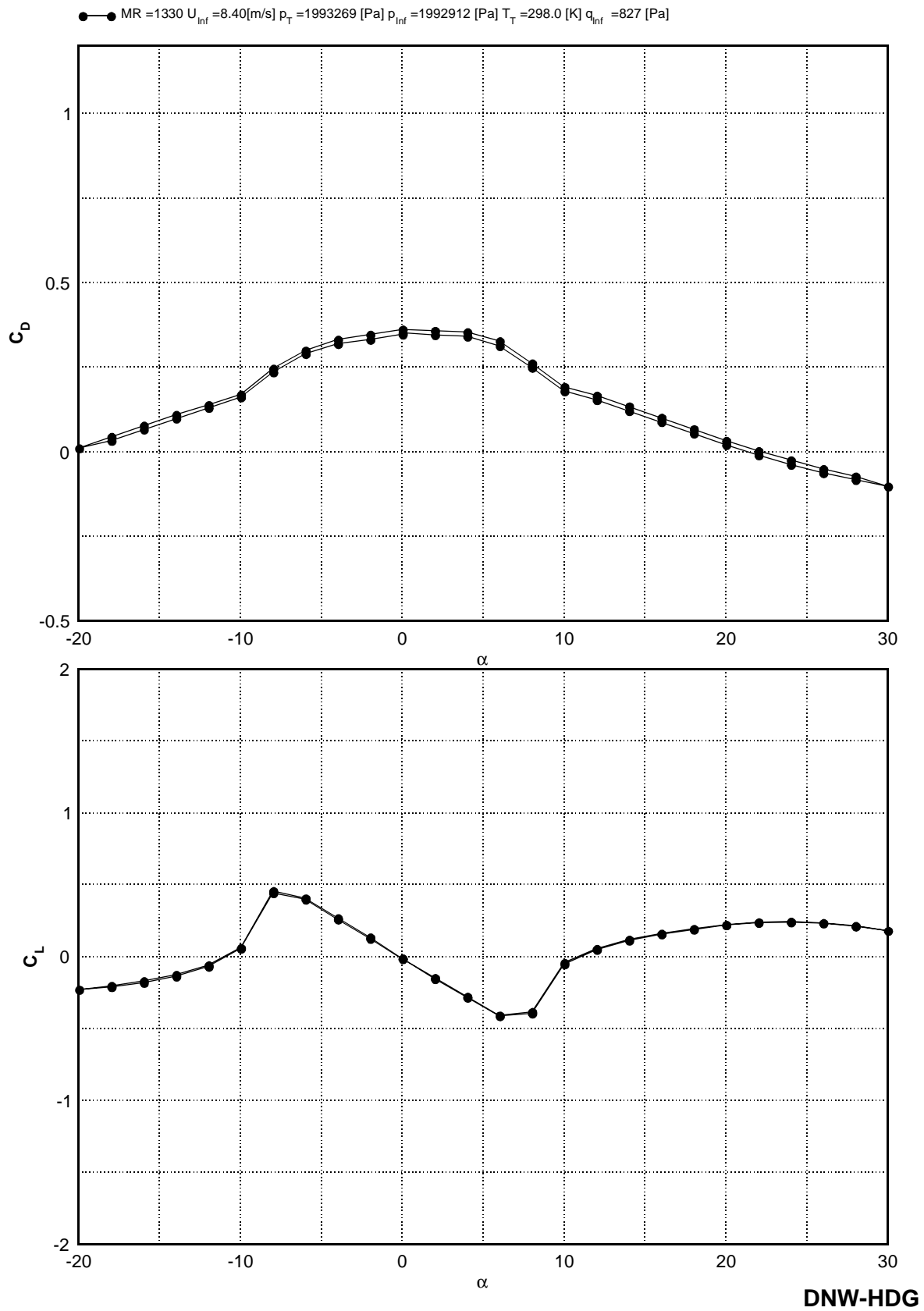


Figure 3 2'nd Cylinder  $Re = 0.302 [Mio]$   $Pk = 5bar$



**Figure 4** 2'nd Cylinder  $Re = 0.404 [\text{Mio}]$   $Pk = 20\text{bar}$

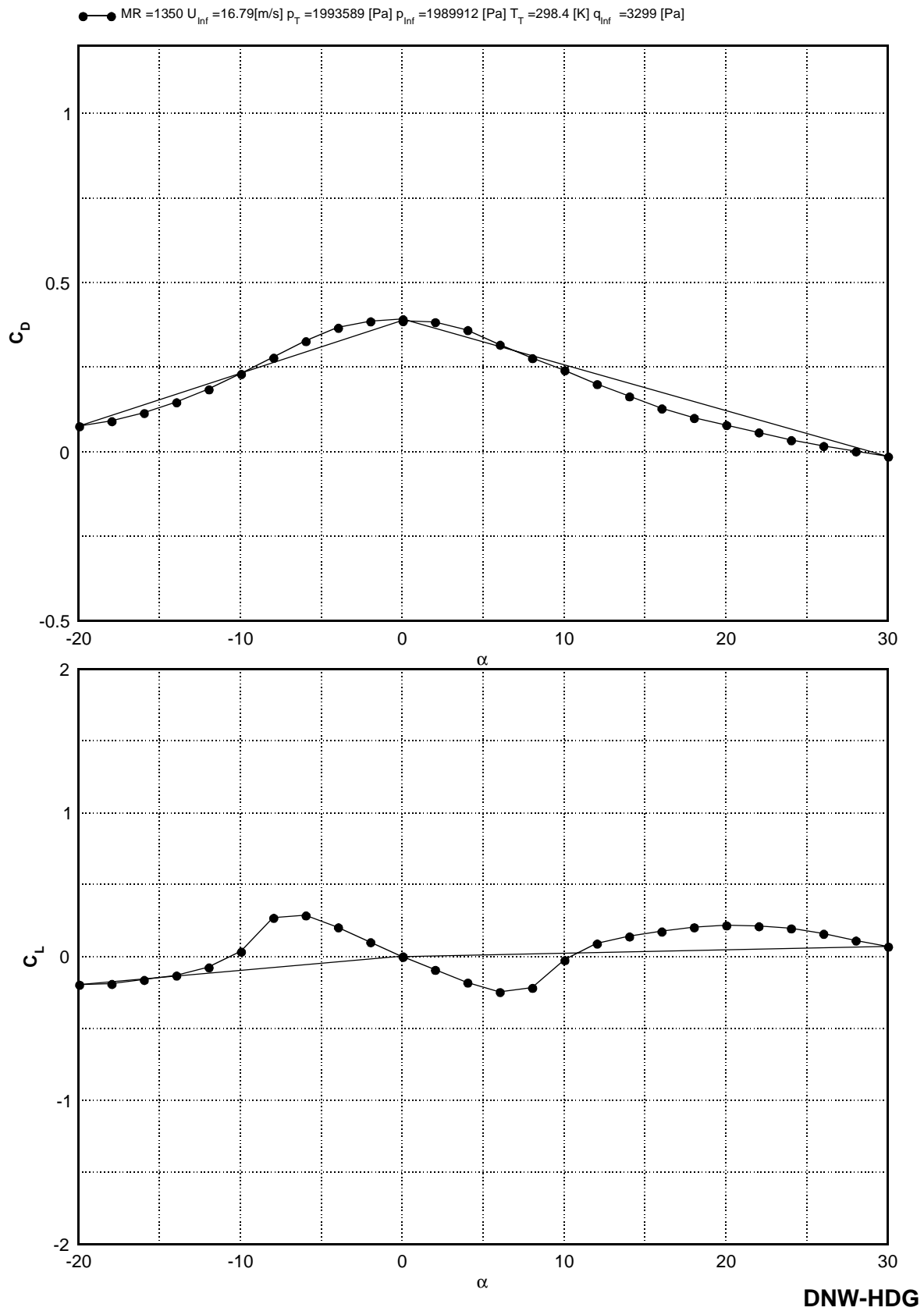


Figure 5 2'nd Cylinder  $Re= 0.806 [\text{Mio}]$   $Pk=20\text{bar}$

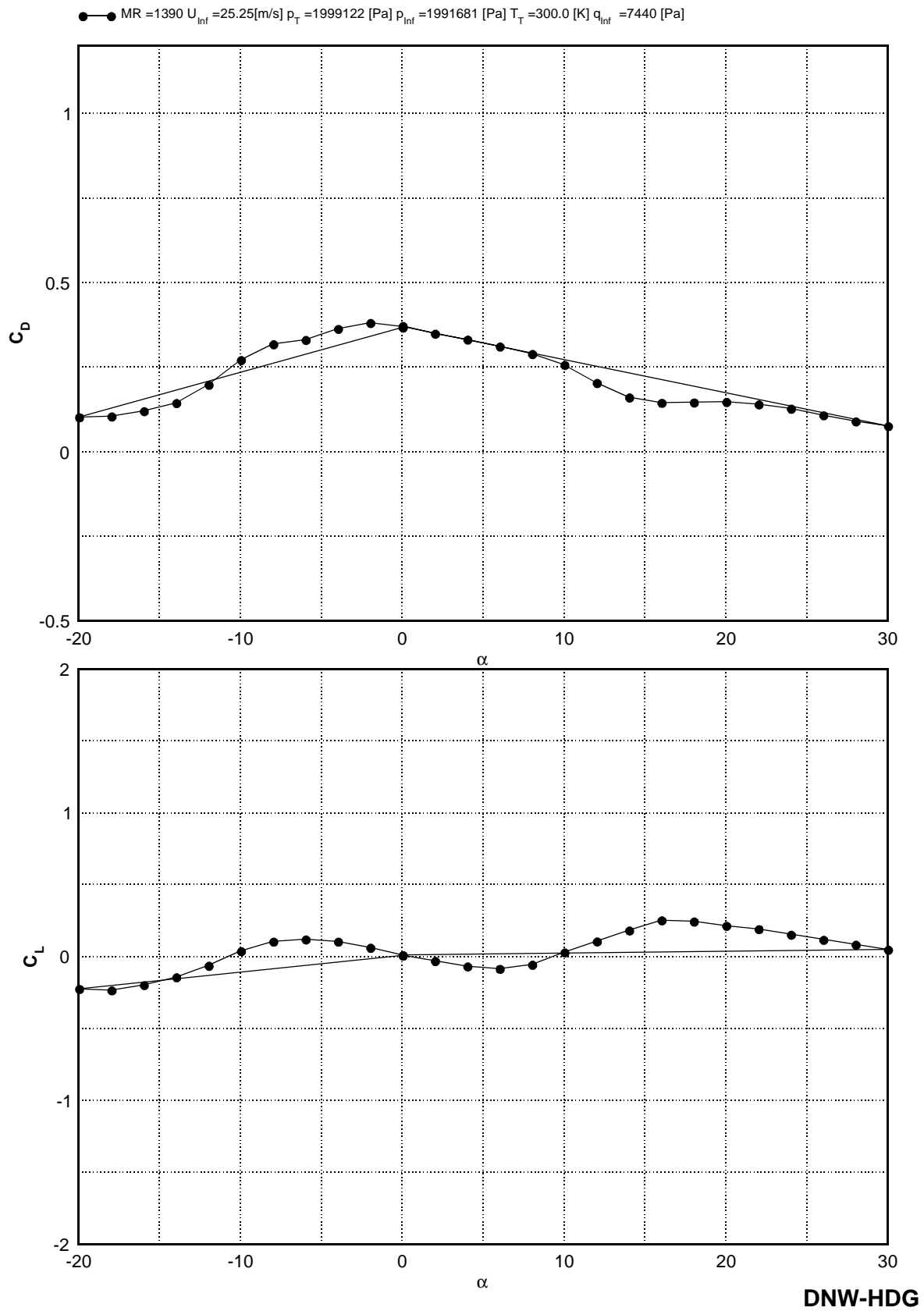


Figure 6 2'nd Cylinder  $Re= 1.204 [\text{Mio}]$   $Pk=20\text{bar}$

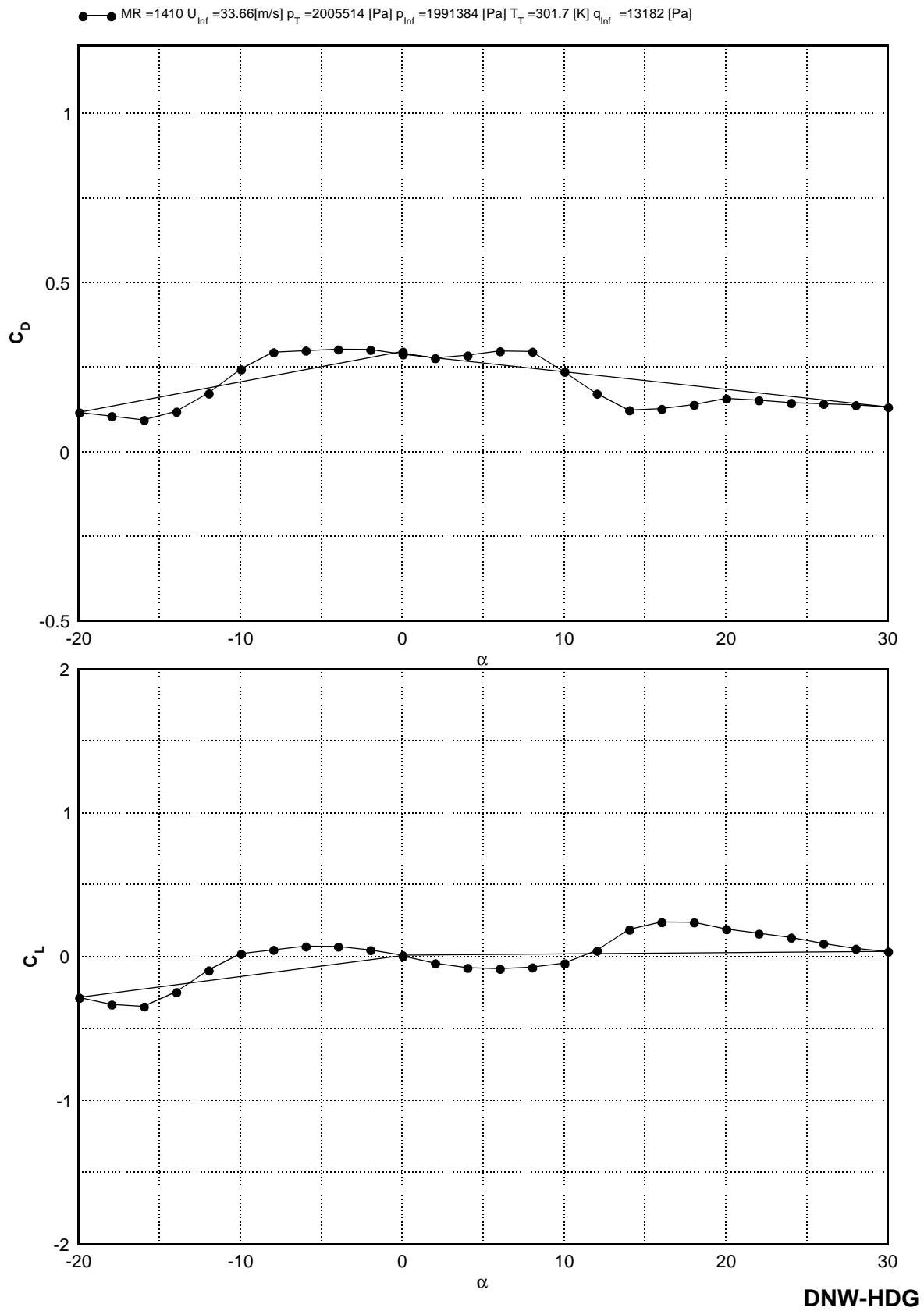
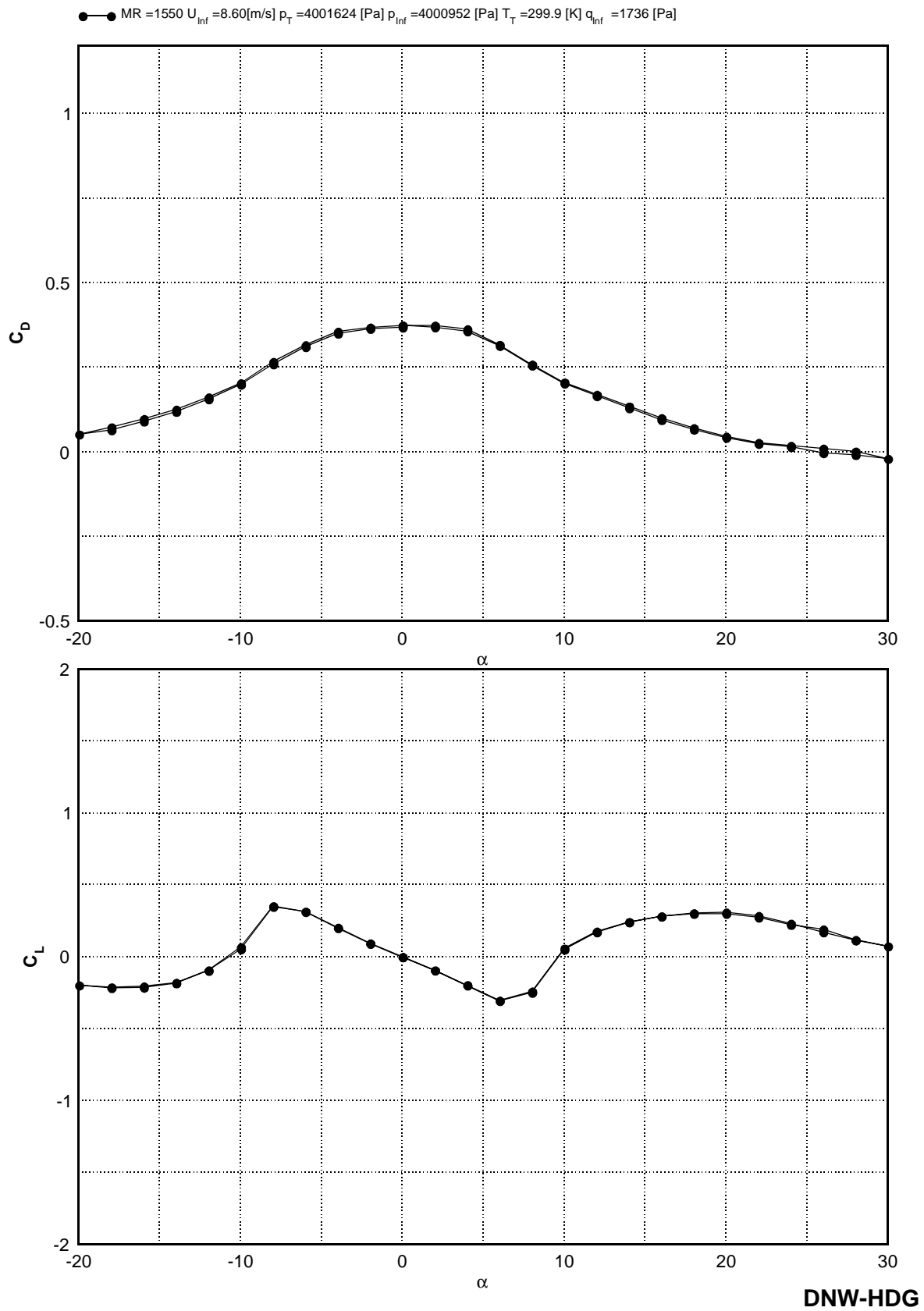


Figure 7 2'nd Cylinder  $Re = 1.594$  [Mio]  $Pk = 20$  bar



**Figure 8** 2'nd Cylinder  $Re = 0.808 [\text{Mio}]$   $Pk = 40\text{bar}$



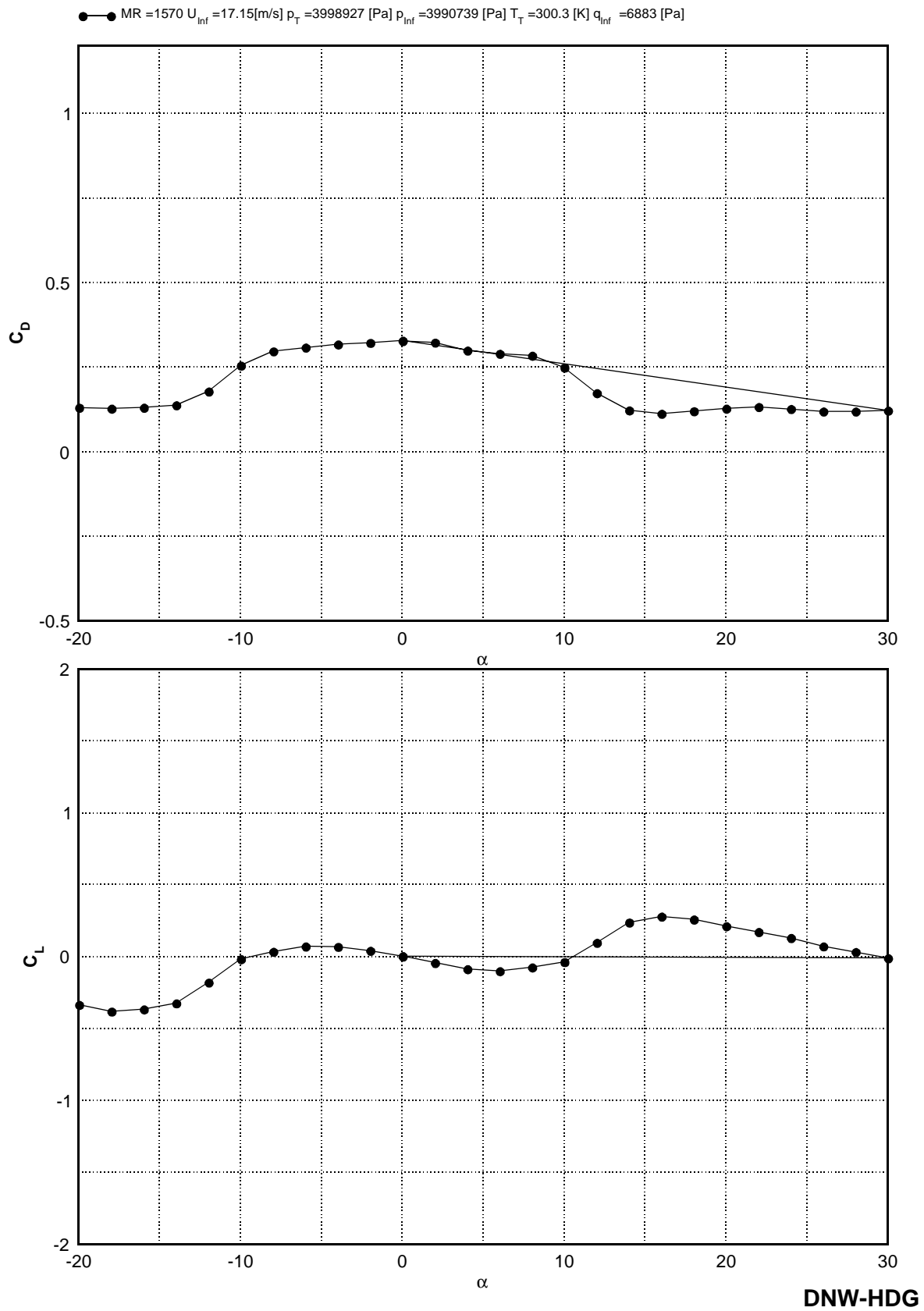
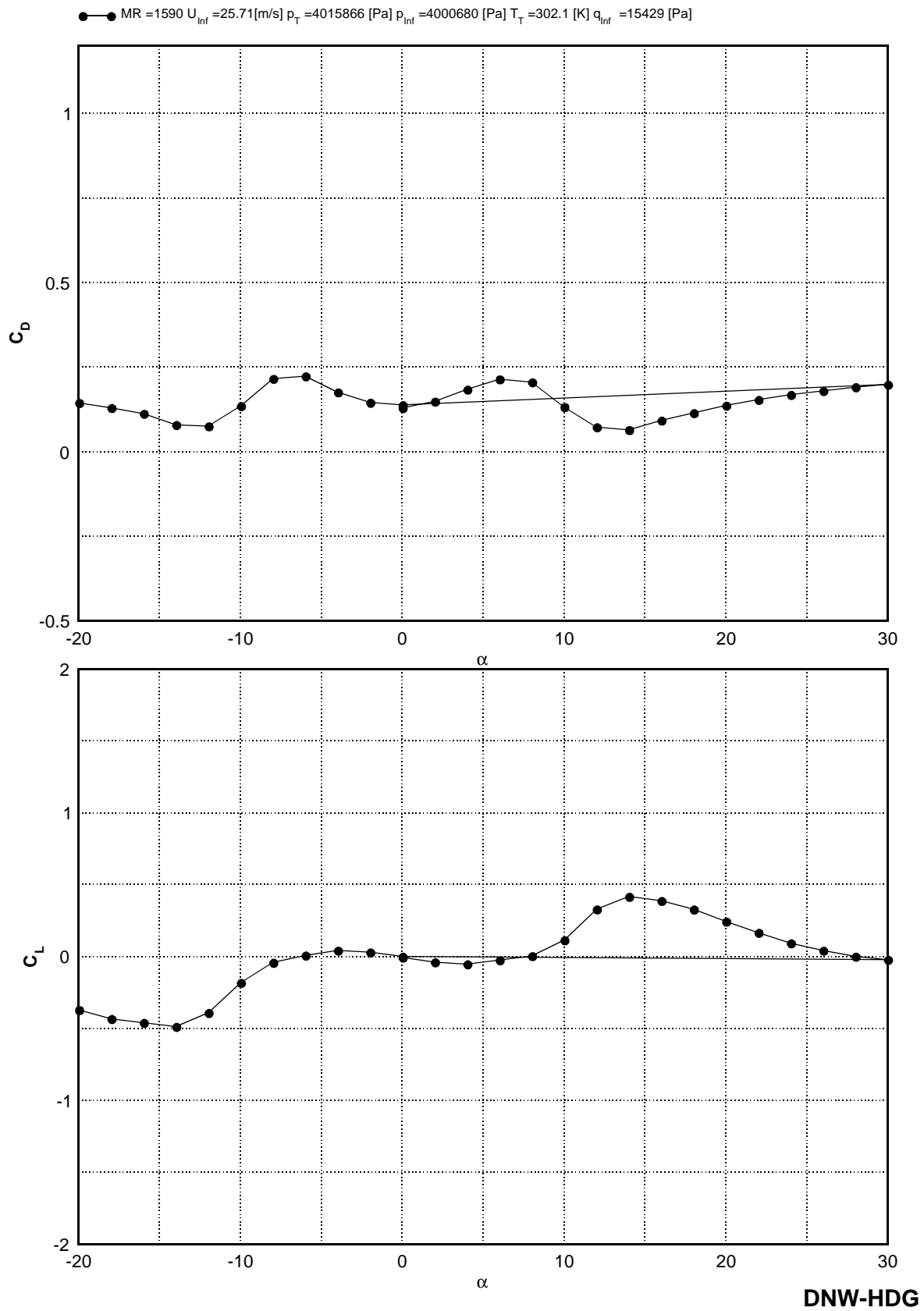
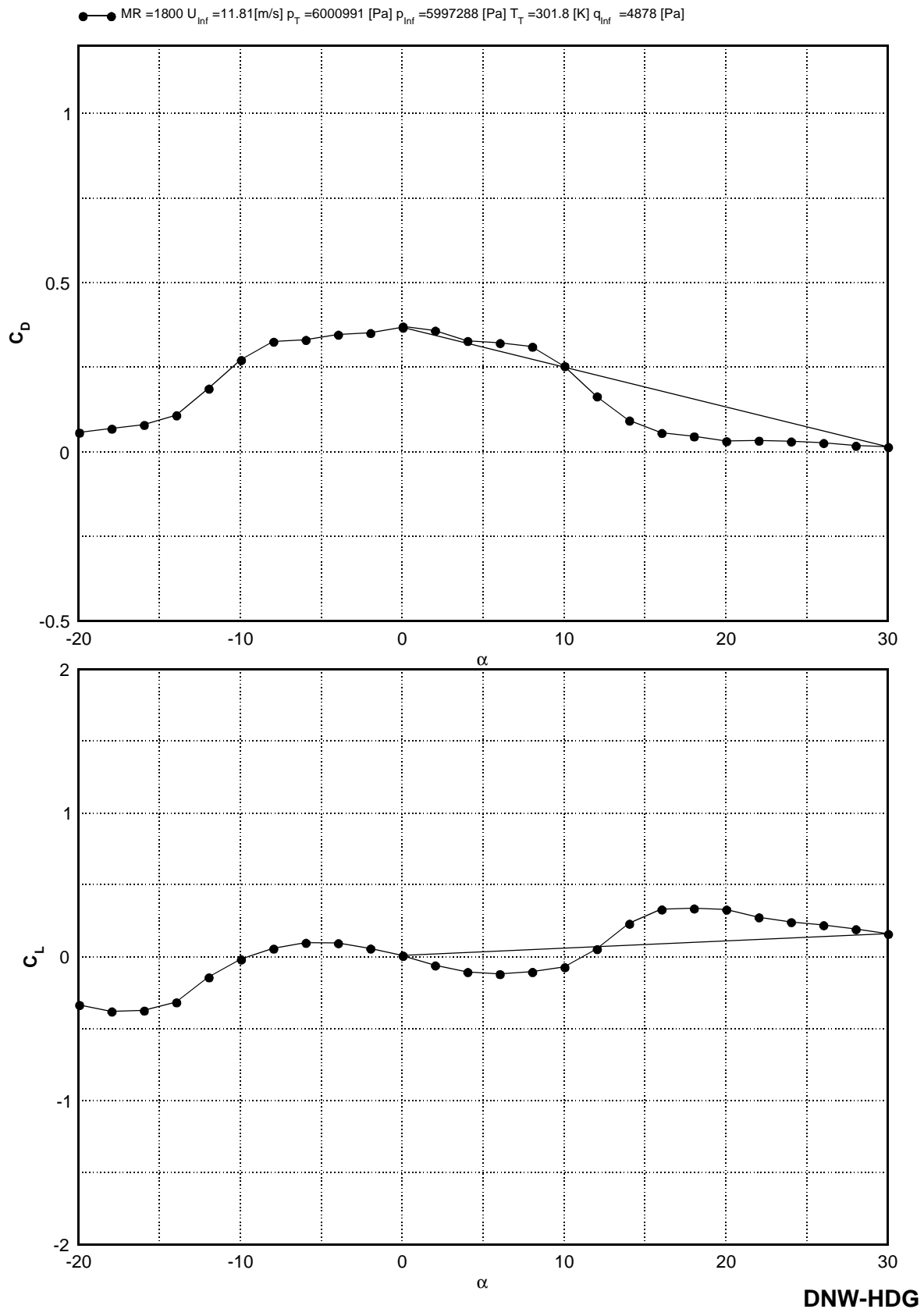


Figure 9 2'nd Cylinder  $Re= 1.606 [\text{Mio}]$   $Pk=40\text{bar}$



**Figure 10** 2'nd Cylinder  $Re = 2.392 [\text{Mio}]$   $Pk = 40\text{bar}$



**Figure 11** 2'nd Cylinder  $Re= 1.612 [\text{Mio}]$   $Pk=60\text{bar}$

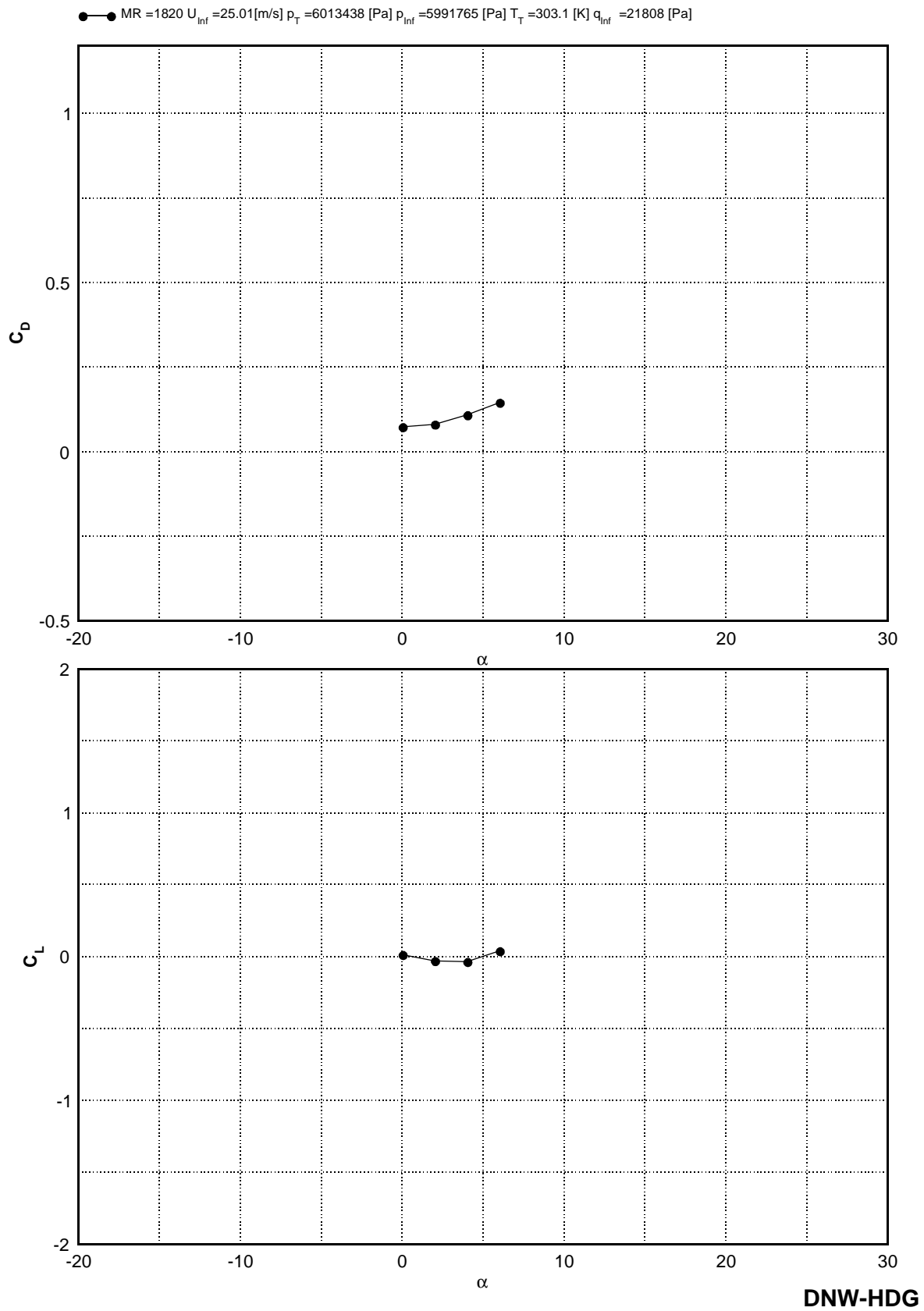


**Figure 12** 2'nd Cylinder  $Re= 3.394 \text{ [Mio]}$   $Pk=60\text{bar}$

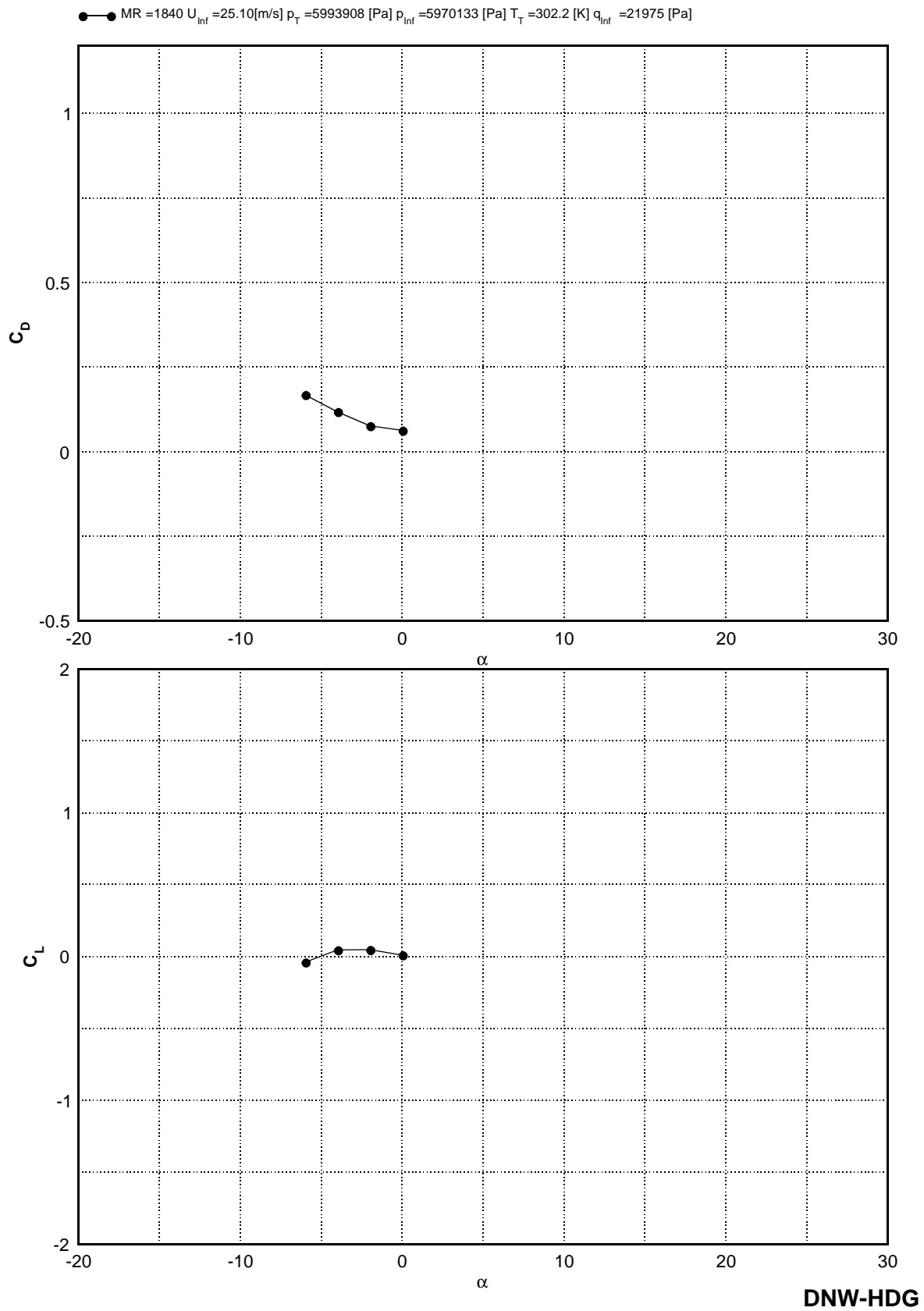


**Figure 13** 2'nd Cylinder  $Re= 3.415 [\text{Mio}]$   $Pk=60\text{bar}$

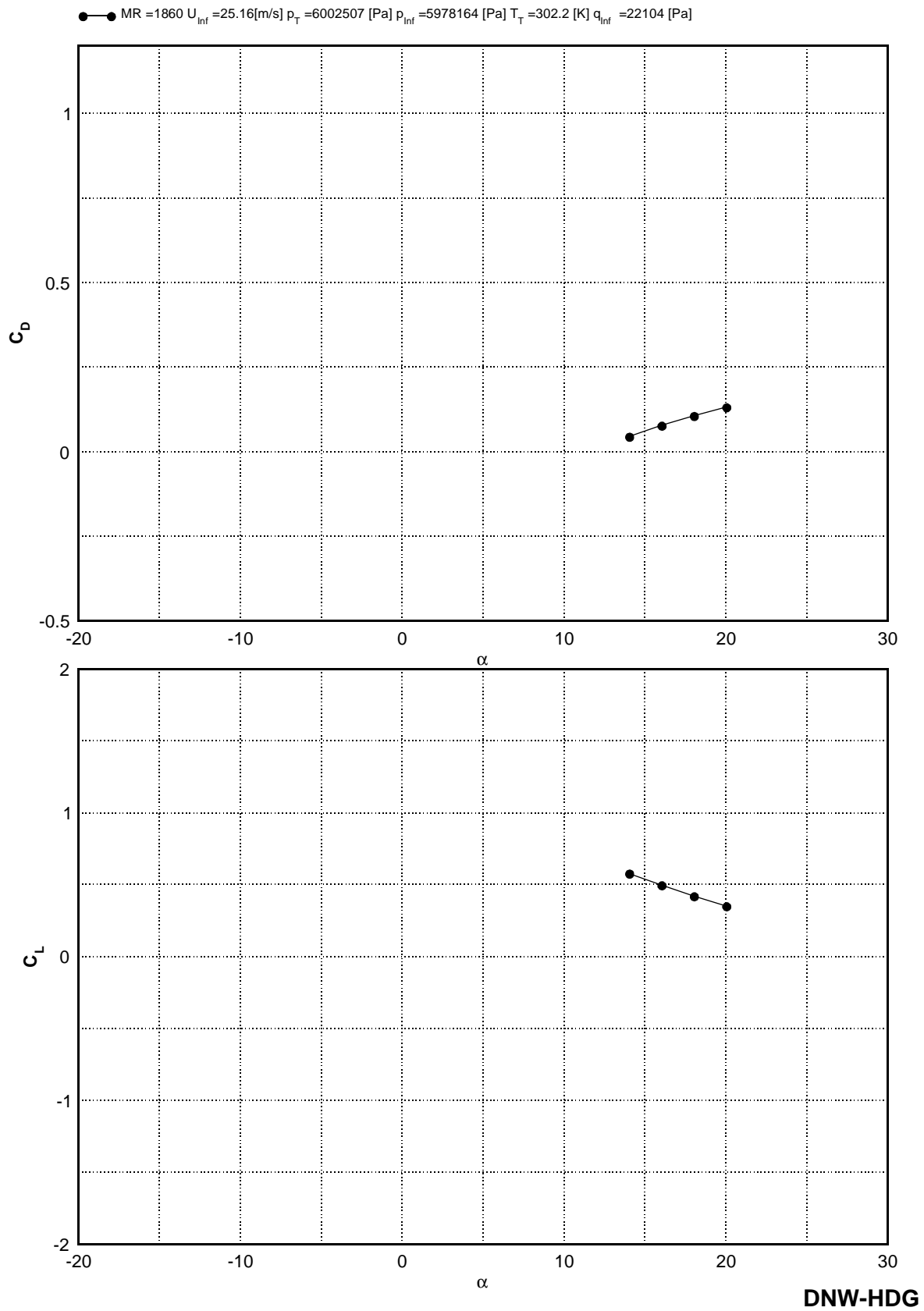


**Figure 14** 2'nd Cylinder  $Re= 3.427$  [Mio]  $Pk=60bar$

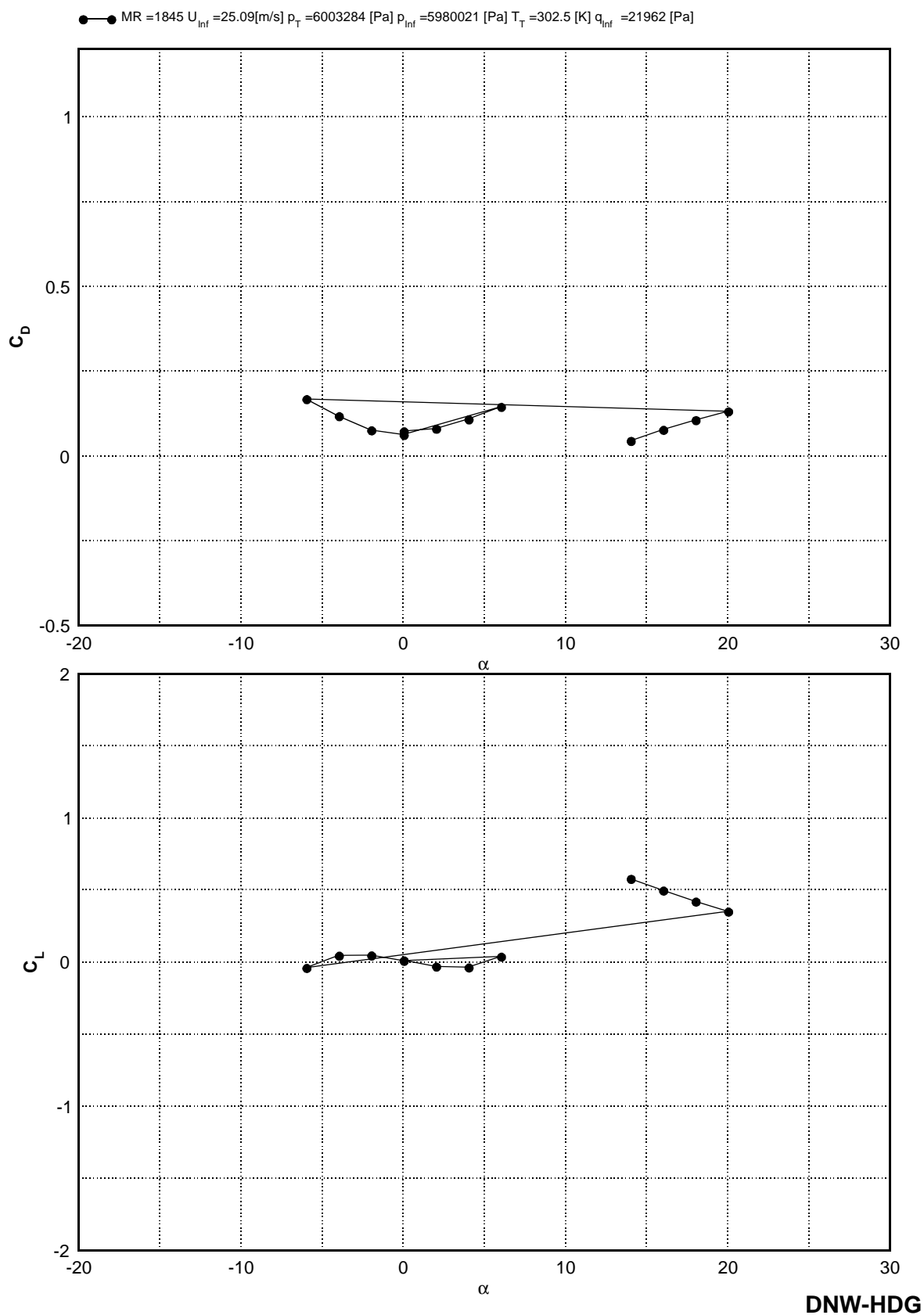
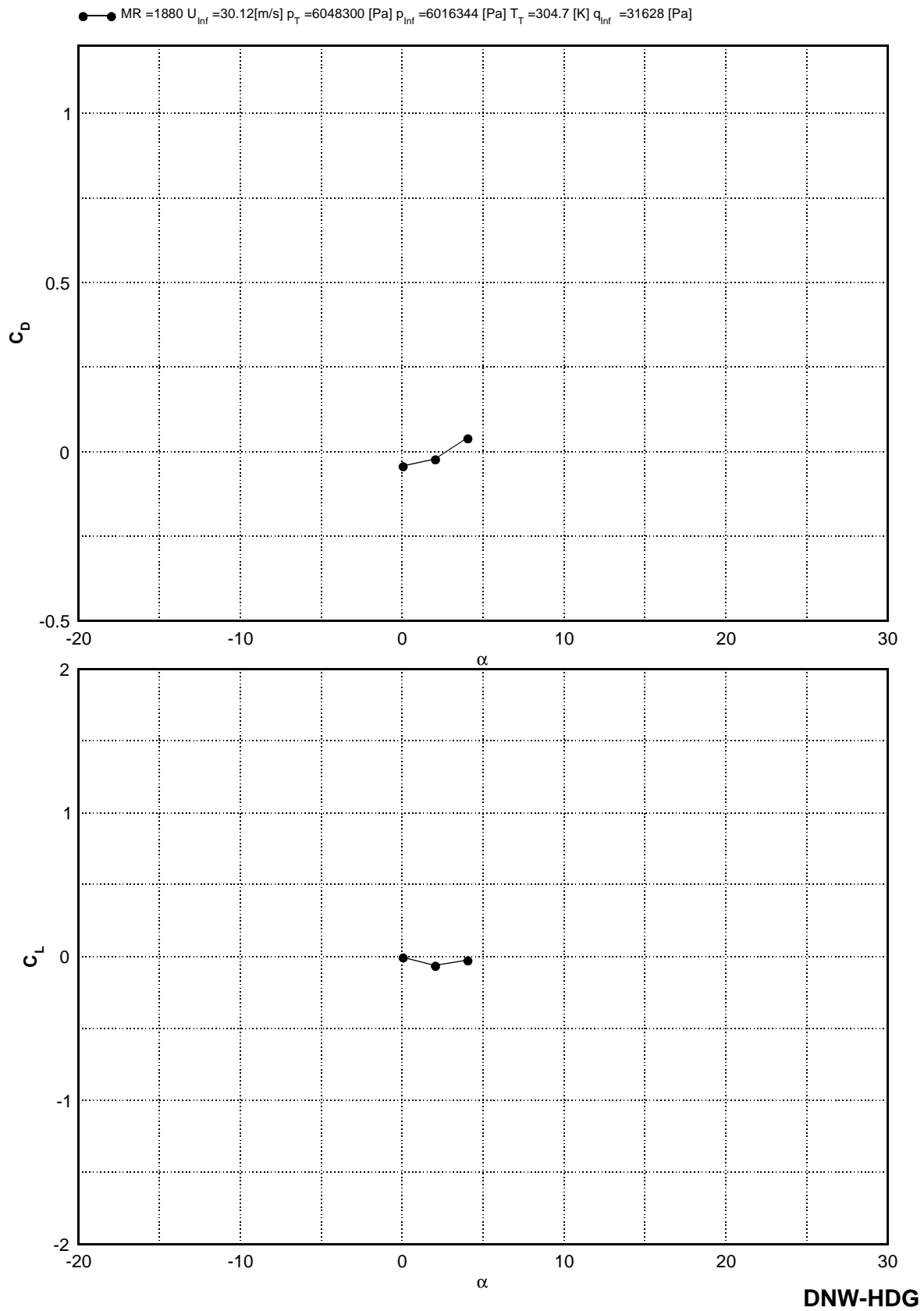


Figure 15 2'nd Cylinder  $Re= 3.412 [\text{Mio}]$   $Pk=60\text{bar}$



**Figure 16** 2'nd Cylinder  $Re= 4.072$  [Mio]  $Pk=60bar$



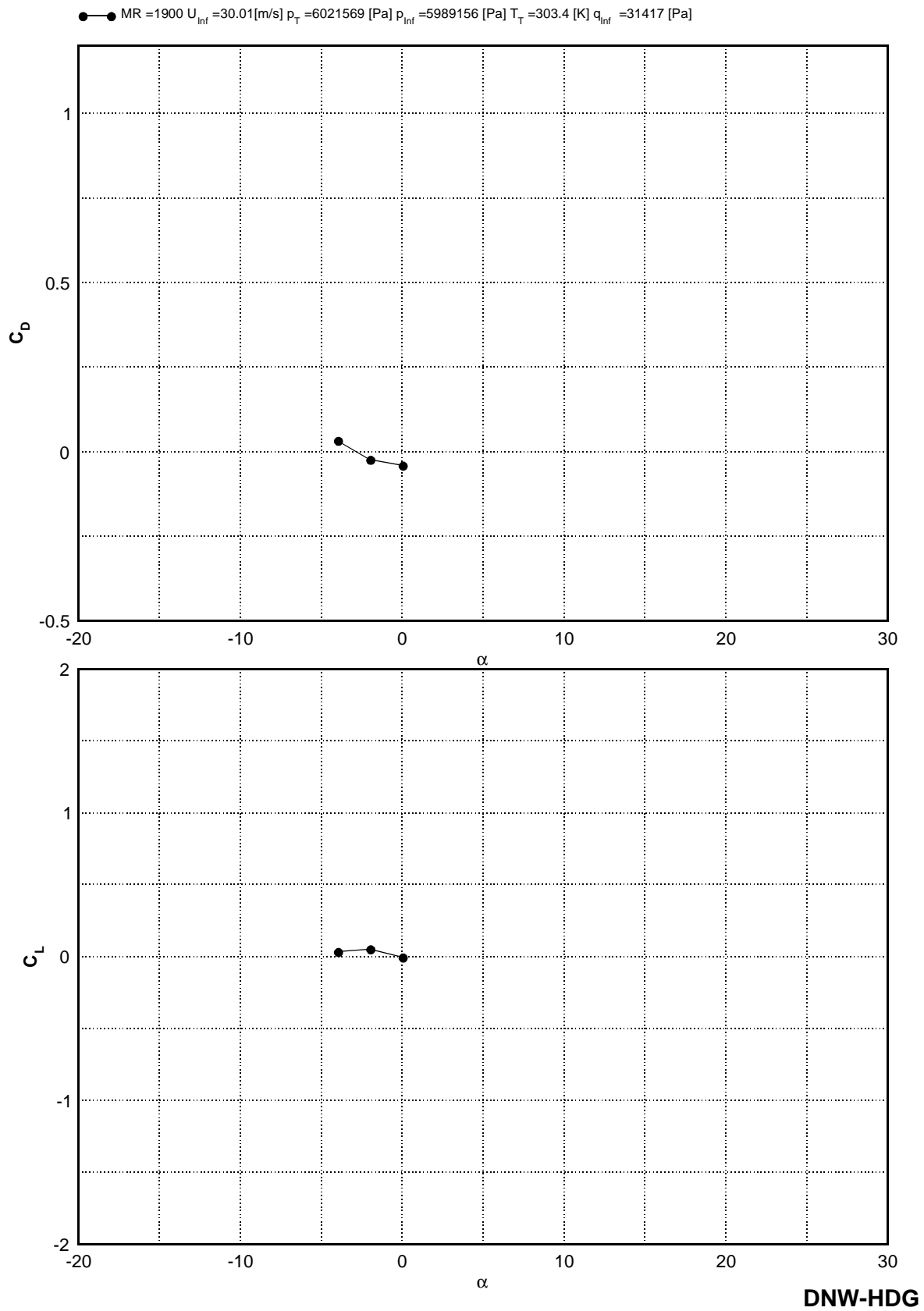
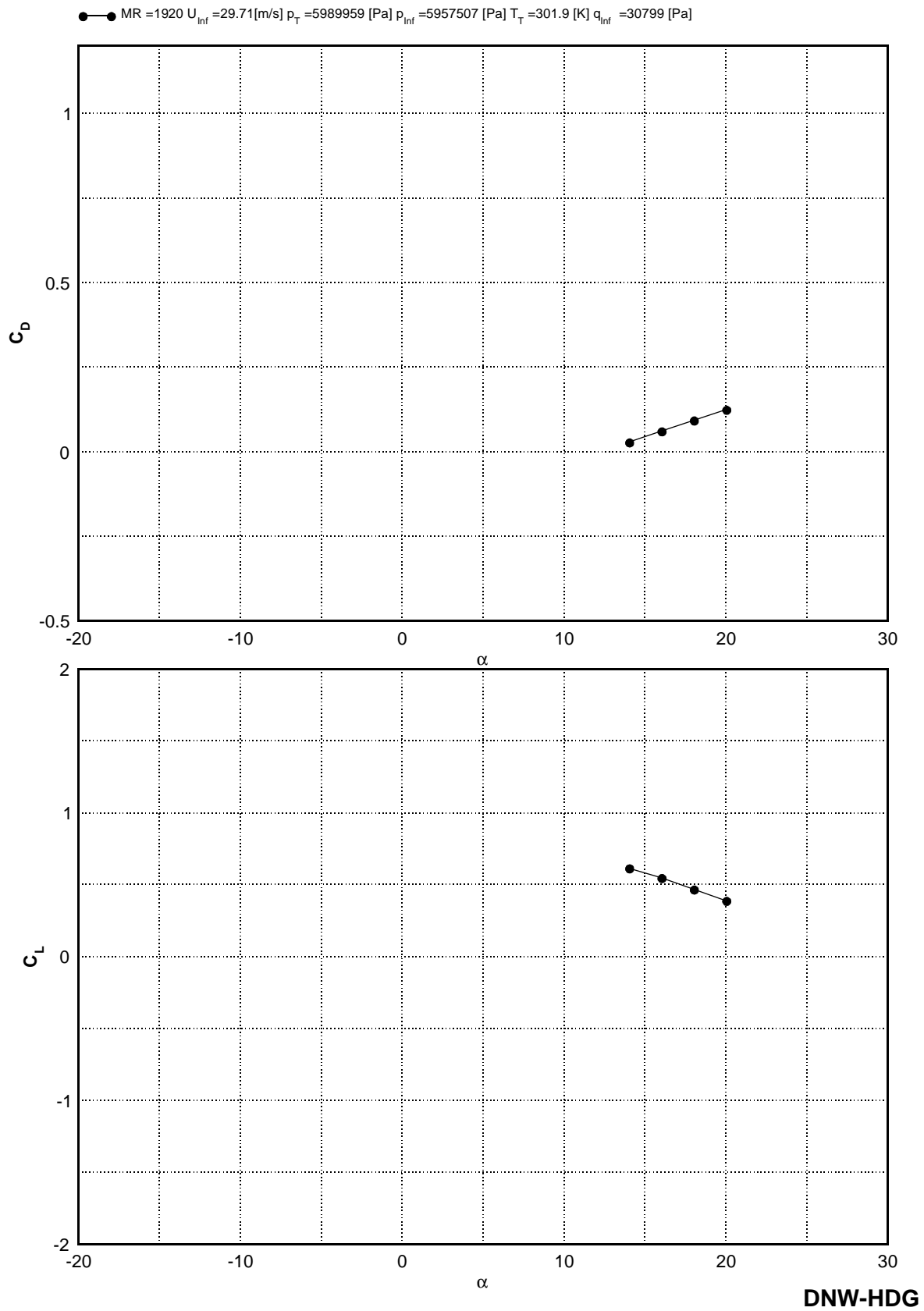
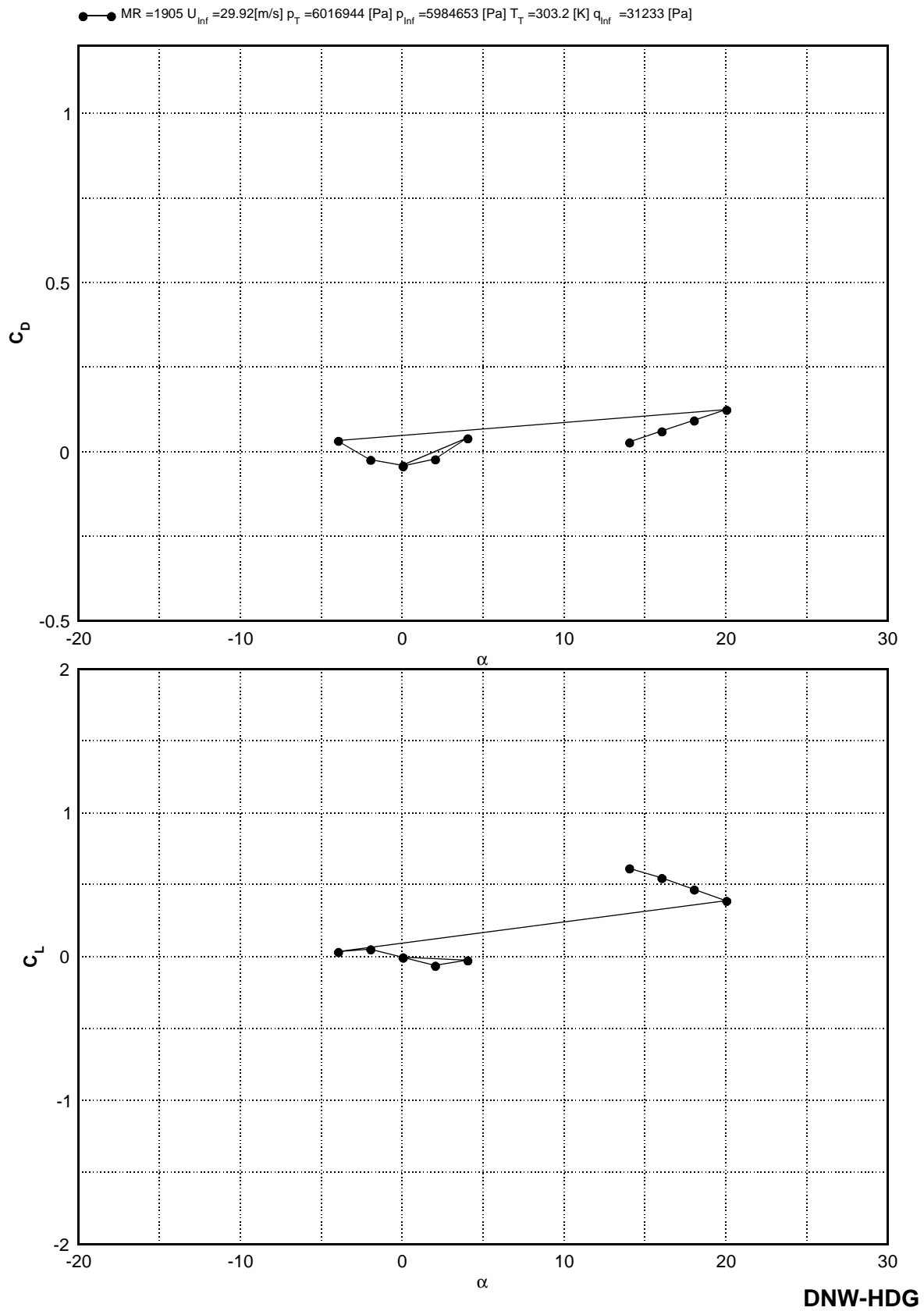


Figure 17 2'nd Cylinder  $Re= 4.071 [\text{Mio}]$   $Pk=60\text{bar}$



**Figure 18** 2'nd Cylinder  $Re= 4.046 [\text{Mio}]$   $Pk=60\text{bar}$



**Figure 19** 2'nd Cylinder  $Re = 4.062$  [Mio]  $Pk=60bar$

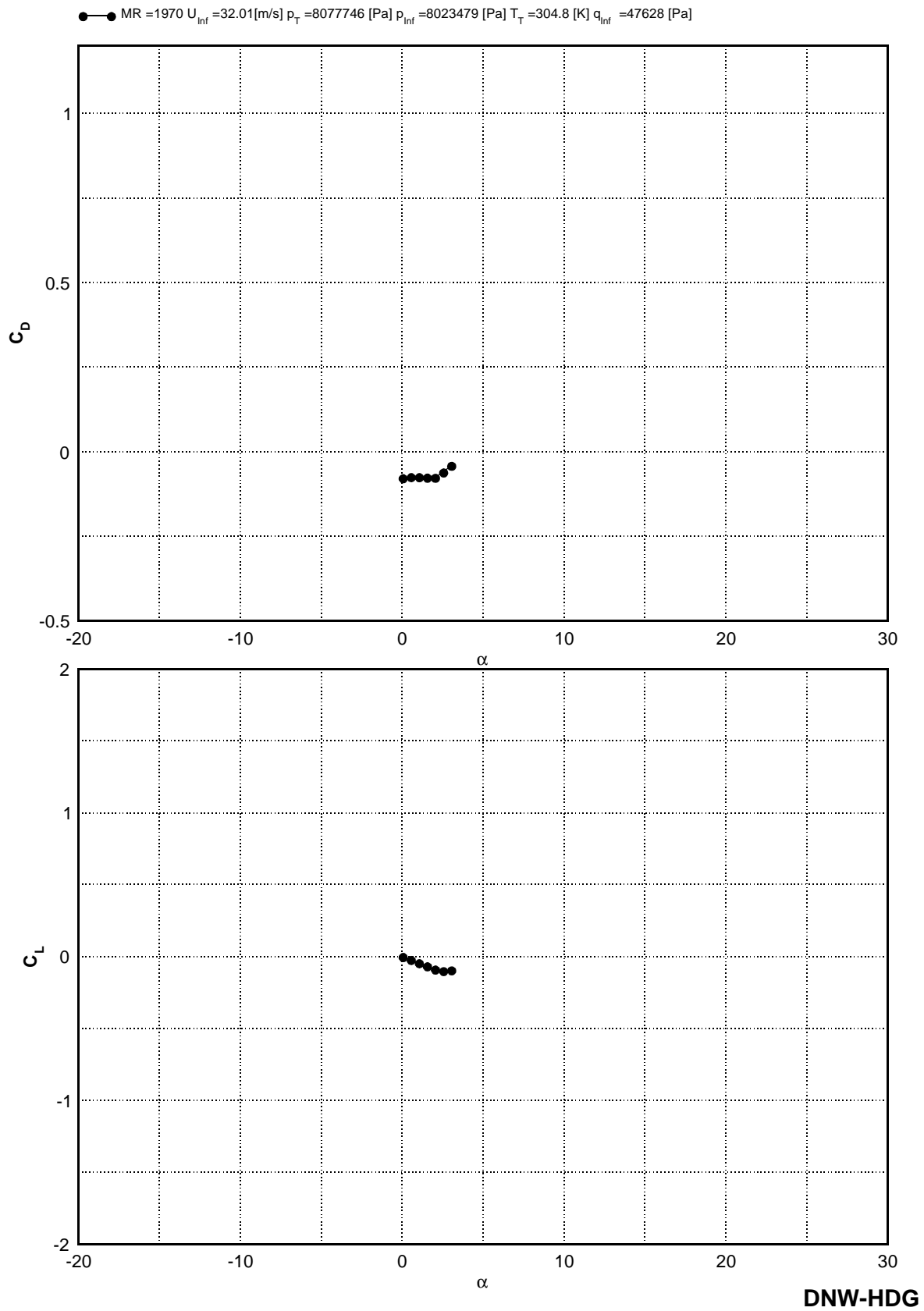


**Figure 20** 2'nd Cylinder  $Re= 5.641 [\text{Mio}]$   $Pk=80\text{bar}$

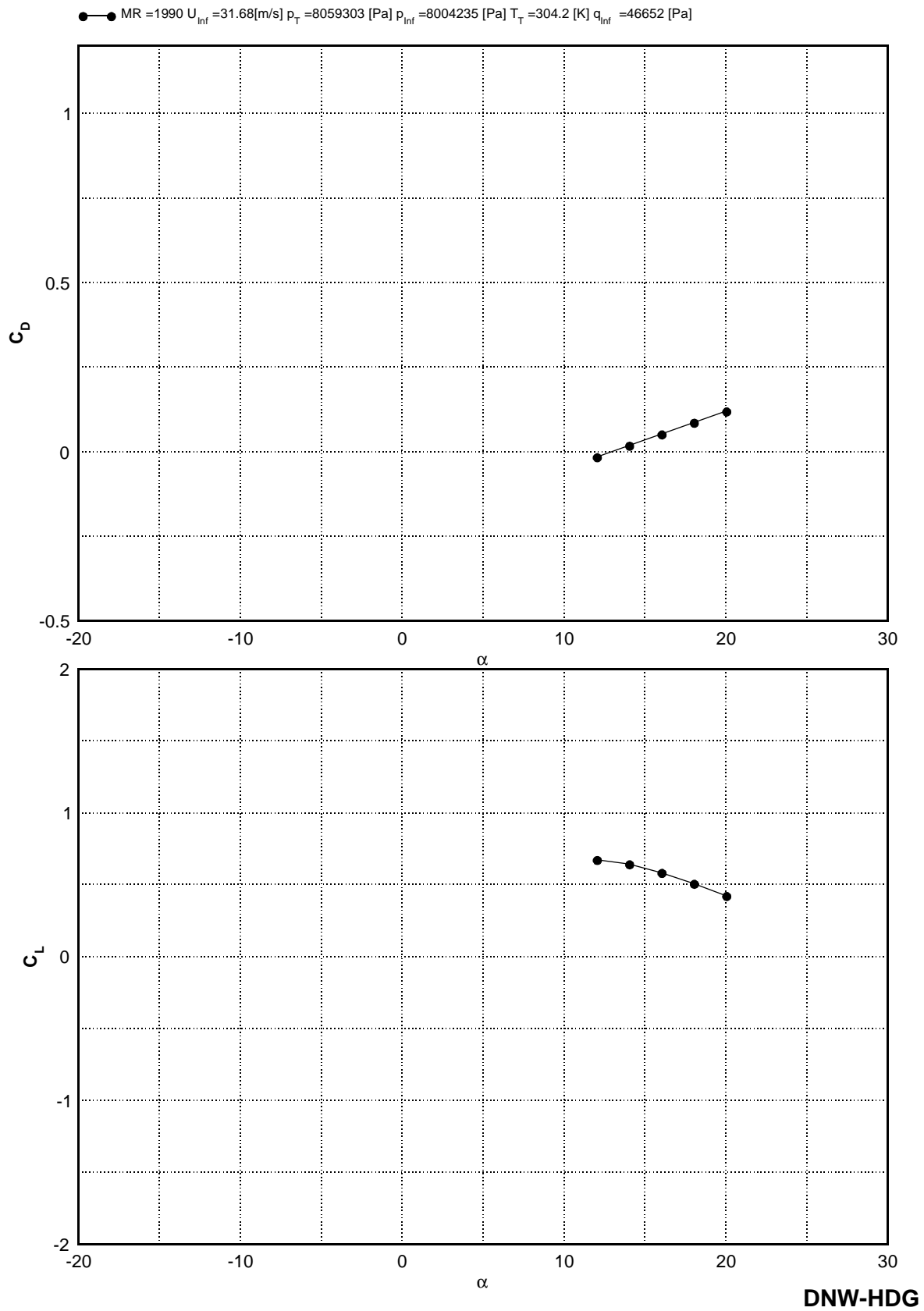


**Figure 21** 2'nd Cylinder  $Re = 5.591 [\text{Mio}]$   $Pk = 80\text{bar}$

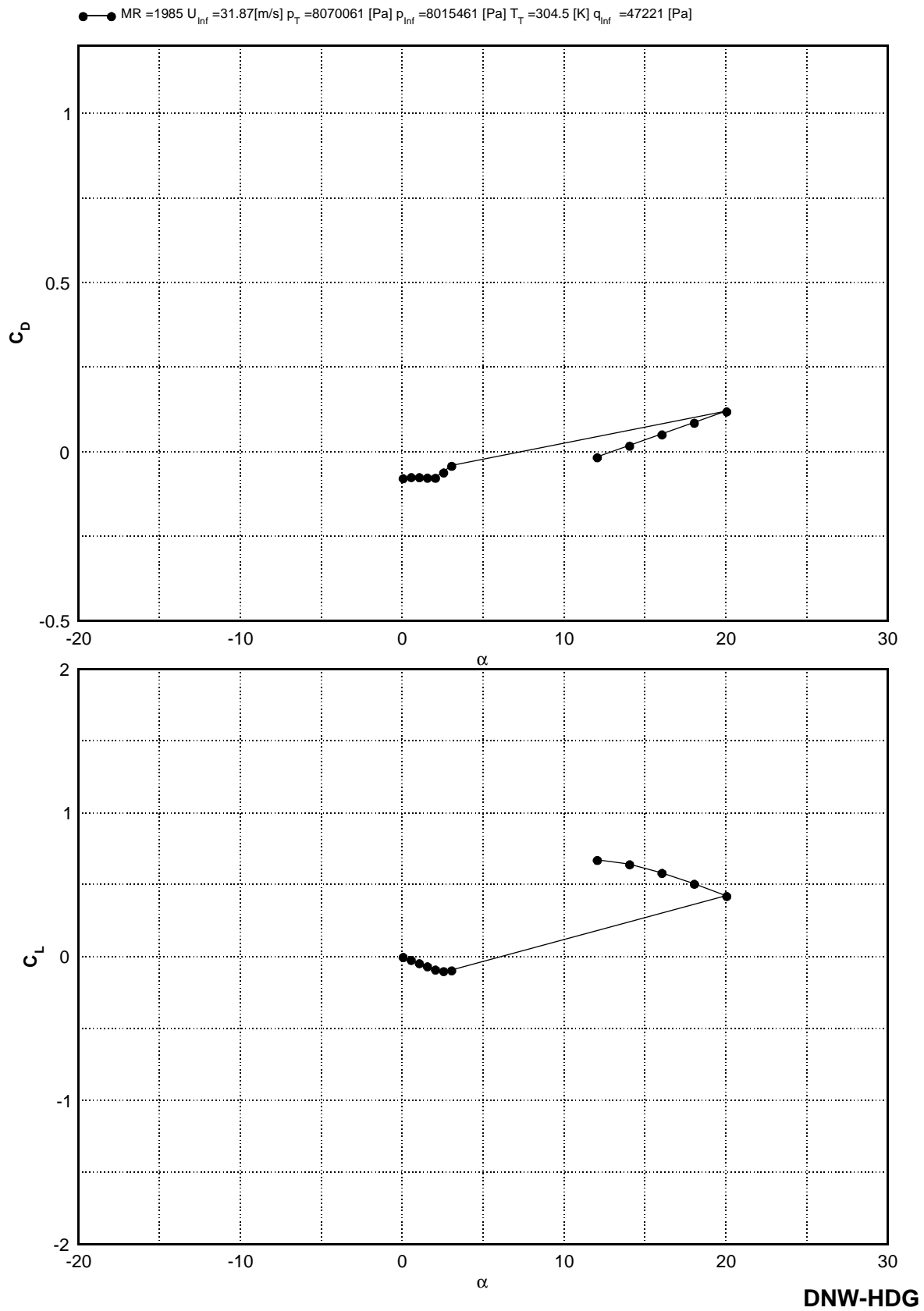


**Figure 22** 2'nd Cylinder  $Re = 5.620 [Mio]$   $Pk = 80bar$

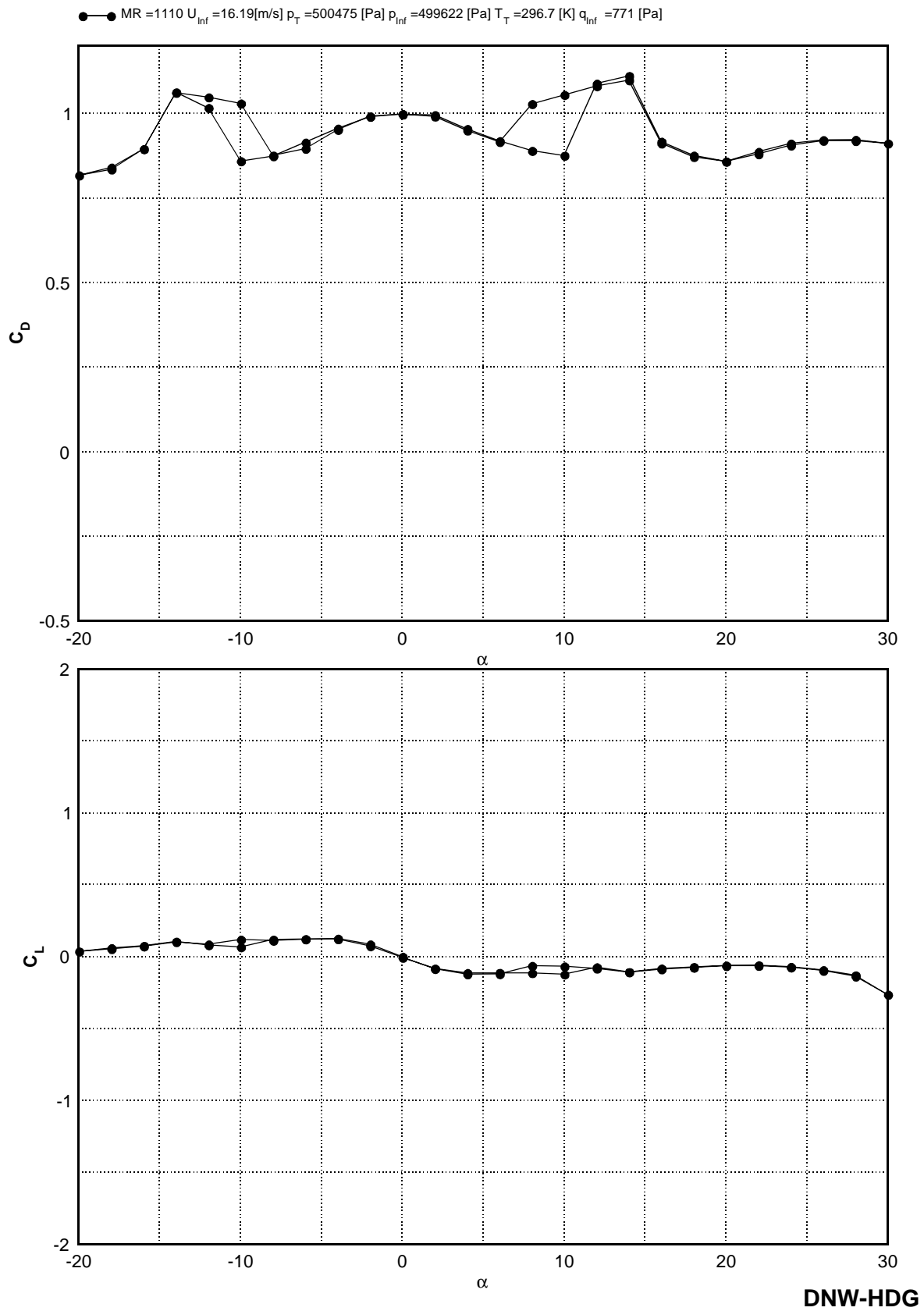


**Figure 23** 1<sup>st</sup> Cylinder  $Re = 0.199 [Mio]$   $Pk = 5bar\_vl$

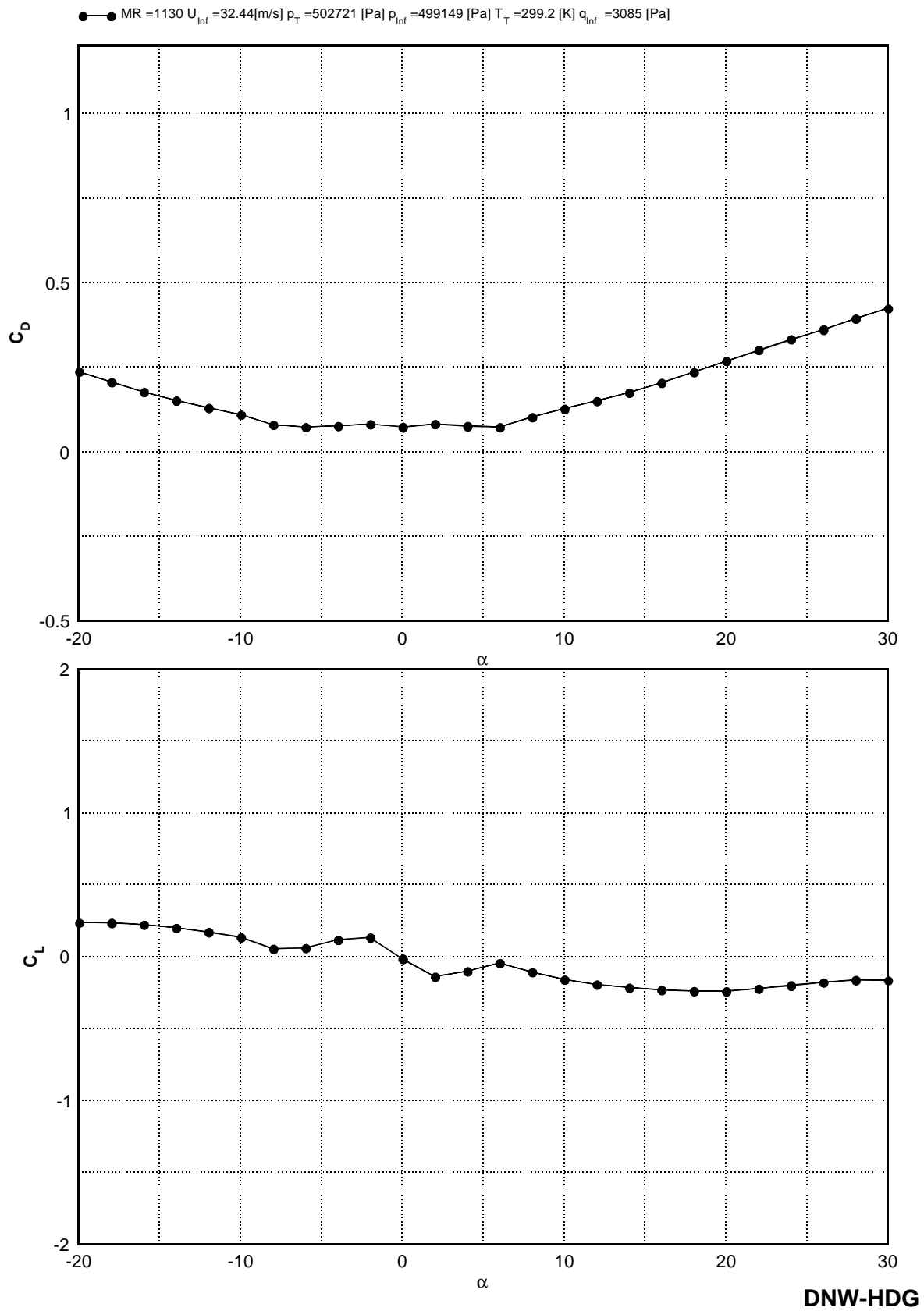


Figure 24 1<sup>st</sup> Cylinder  $Re = 0.395$  [Mio]  $Pk = 5bar\_vl$



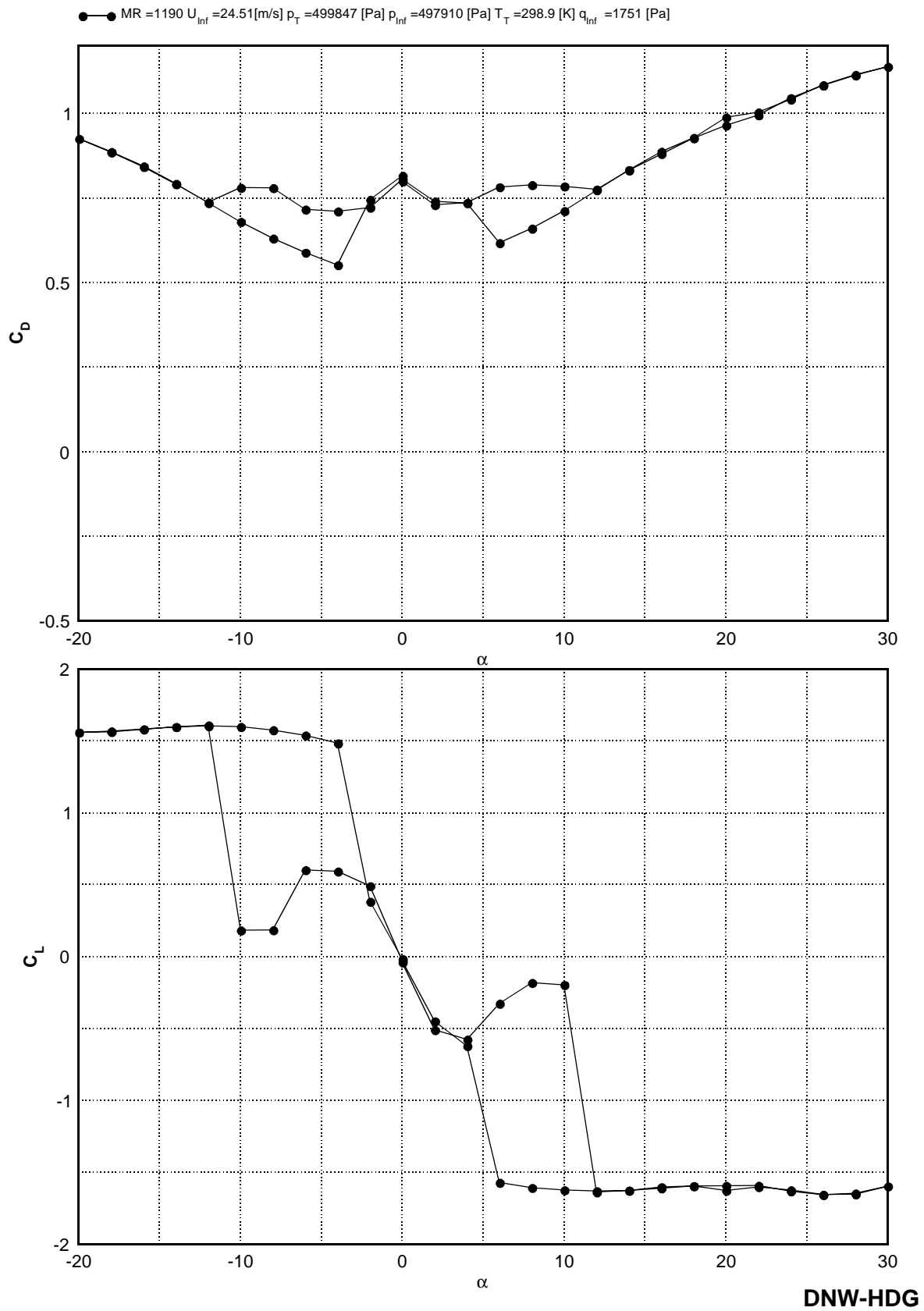


Figure 25 1<sup>st</sup> Cylinder  $Re = 0.297$  [Mio]  $Pk = 5bar\_vl$

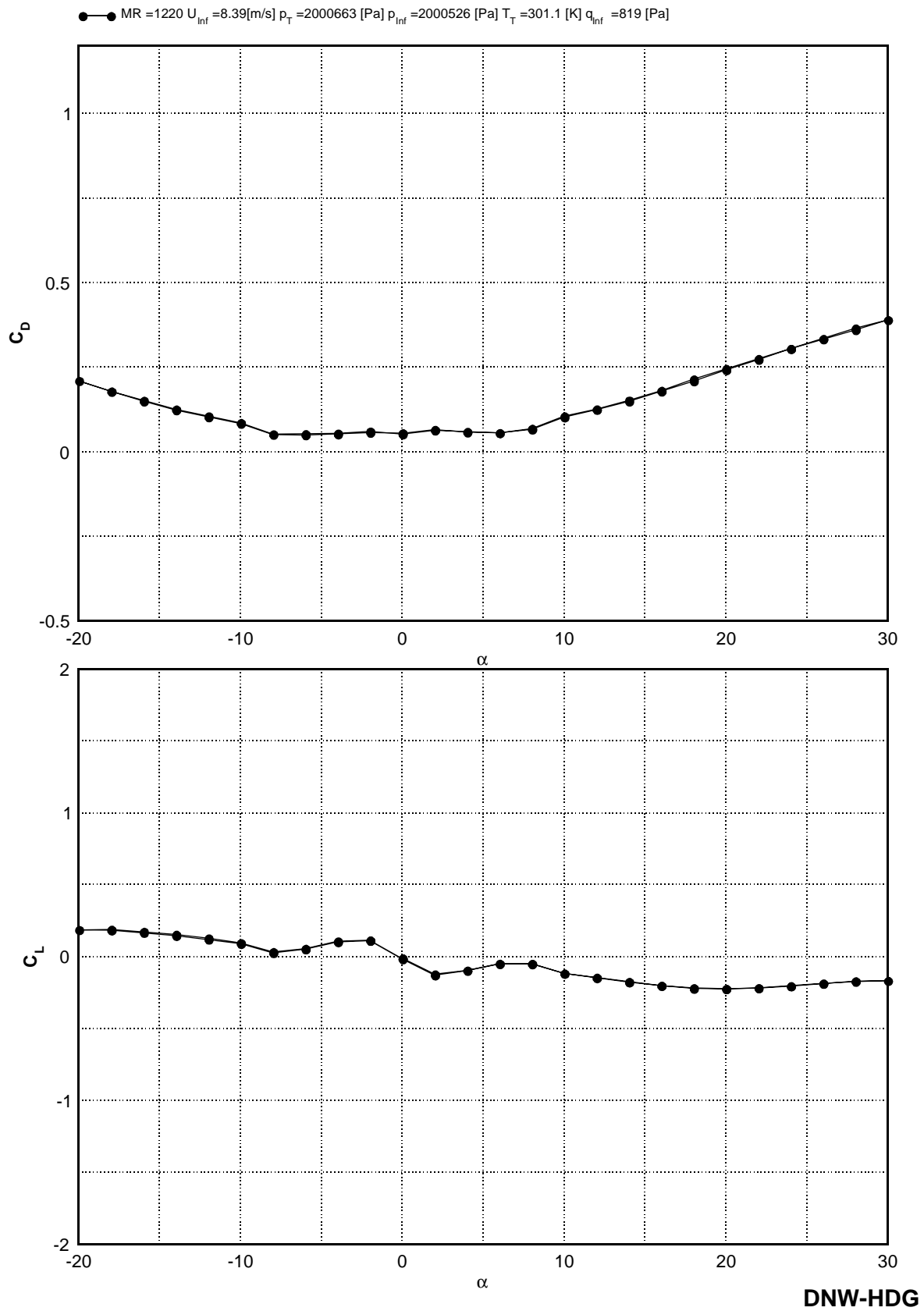


Figure 26 1<sup>st</sup> Cylinder  $Re = 0.398 [\text{Mio}]$  Pk=20bar\_vl

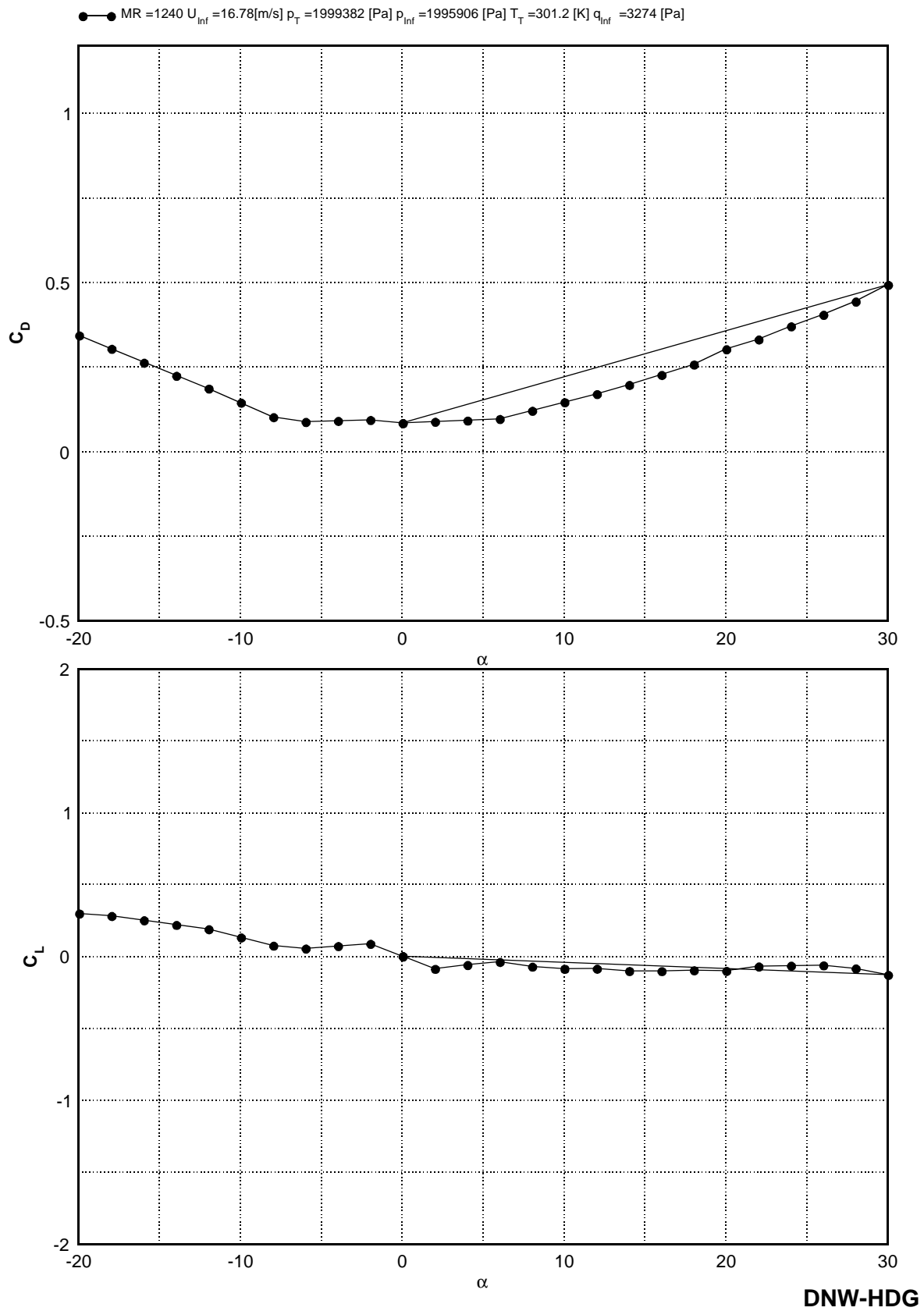


Figure 27 1<sup>st</sup> Cylinder  $Re=0.795$  [Mio] Pk=20bar\_vl

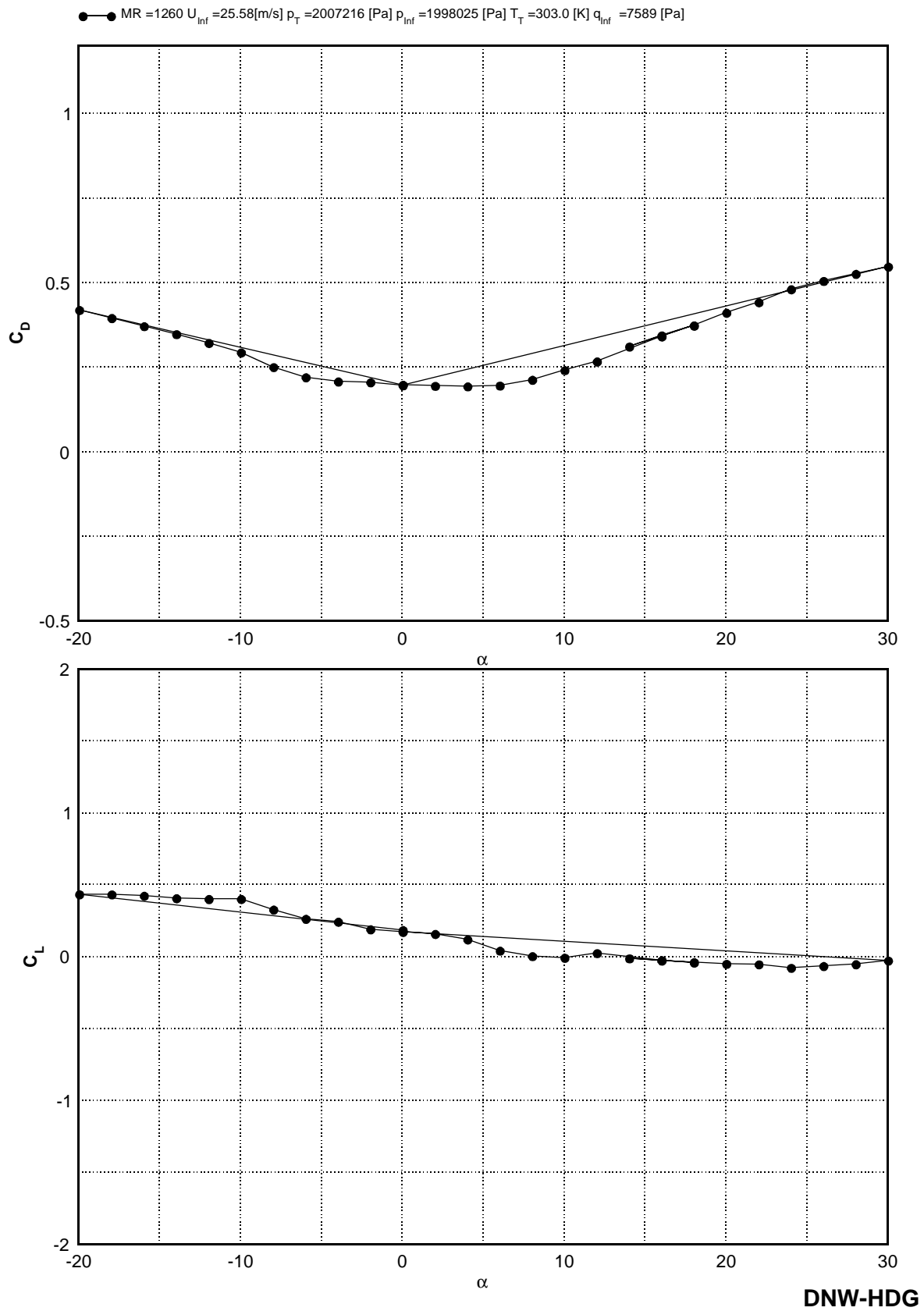
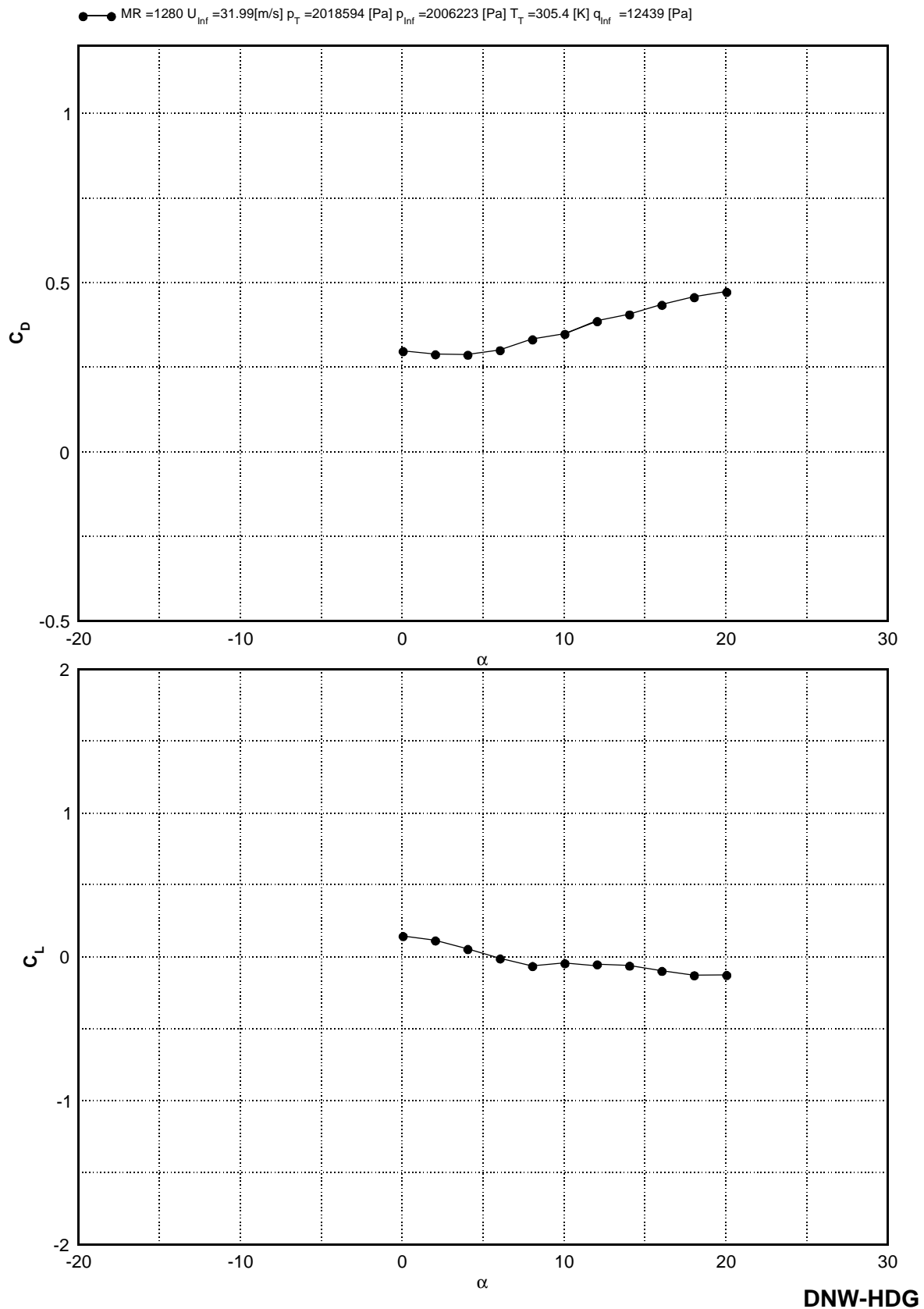


Figure 28 1<sup>st</sup> Cylinder  $Re = 1.204 [\text{Mio}]$  Pk=20bar\_vl



**Figure 29** 1<sup>st</sup> Cylinder  $Re=1.493 [\text{Mio}]$  Pk=20bar\_vl

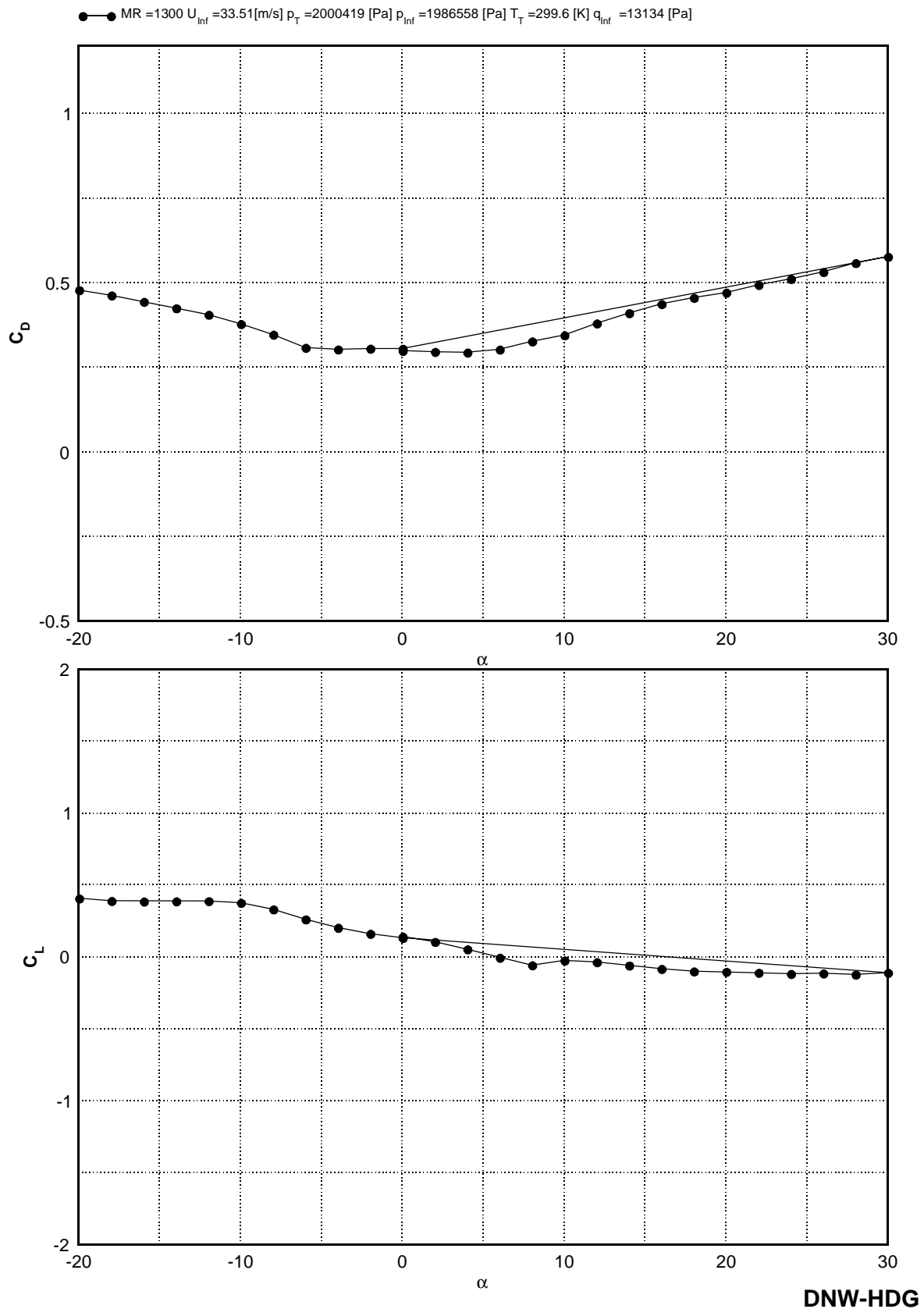
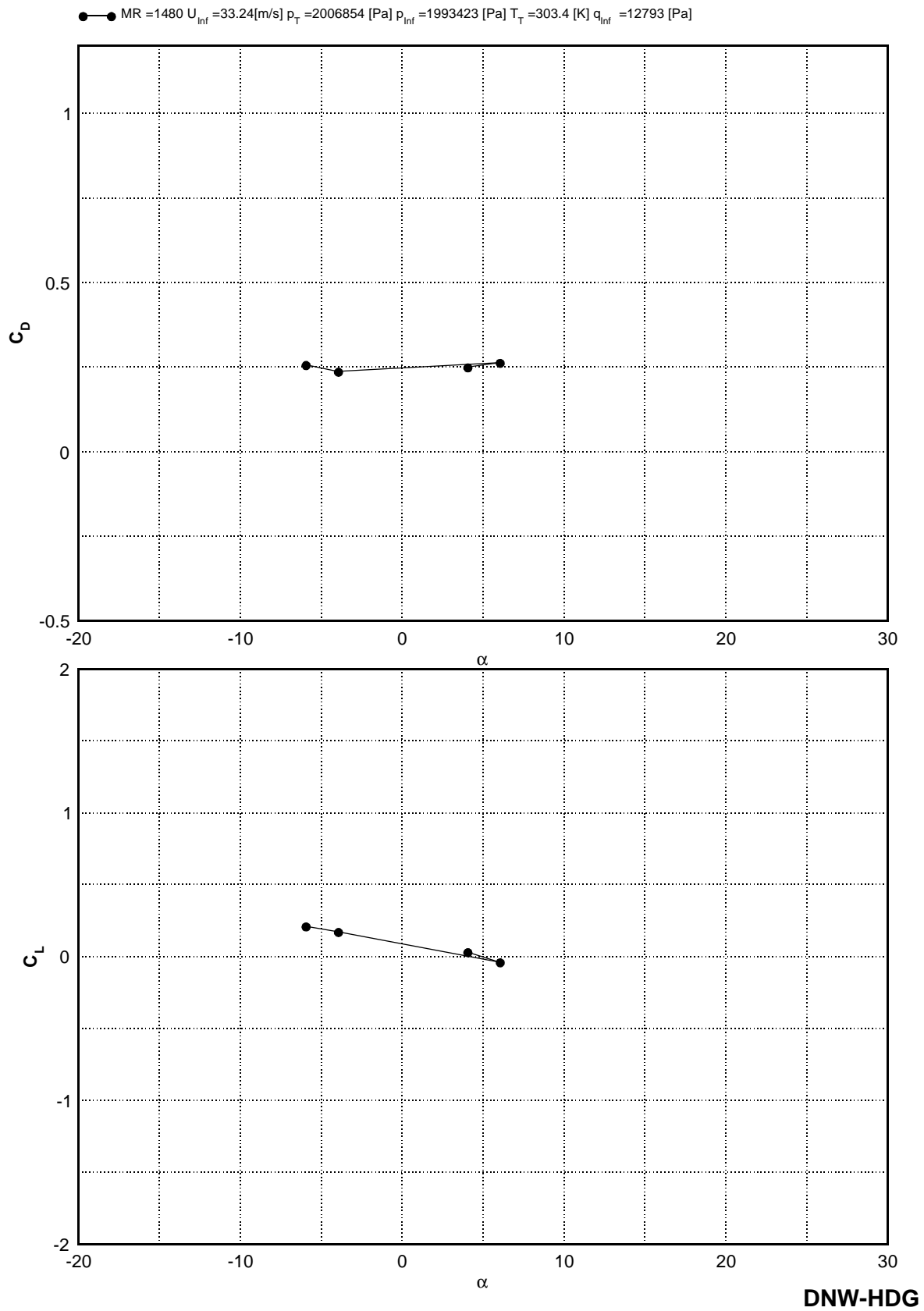
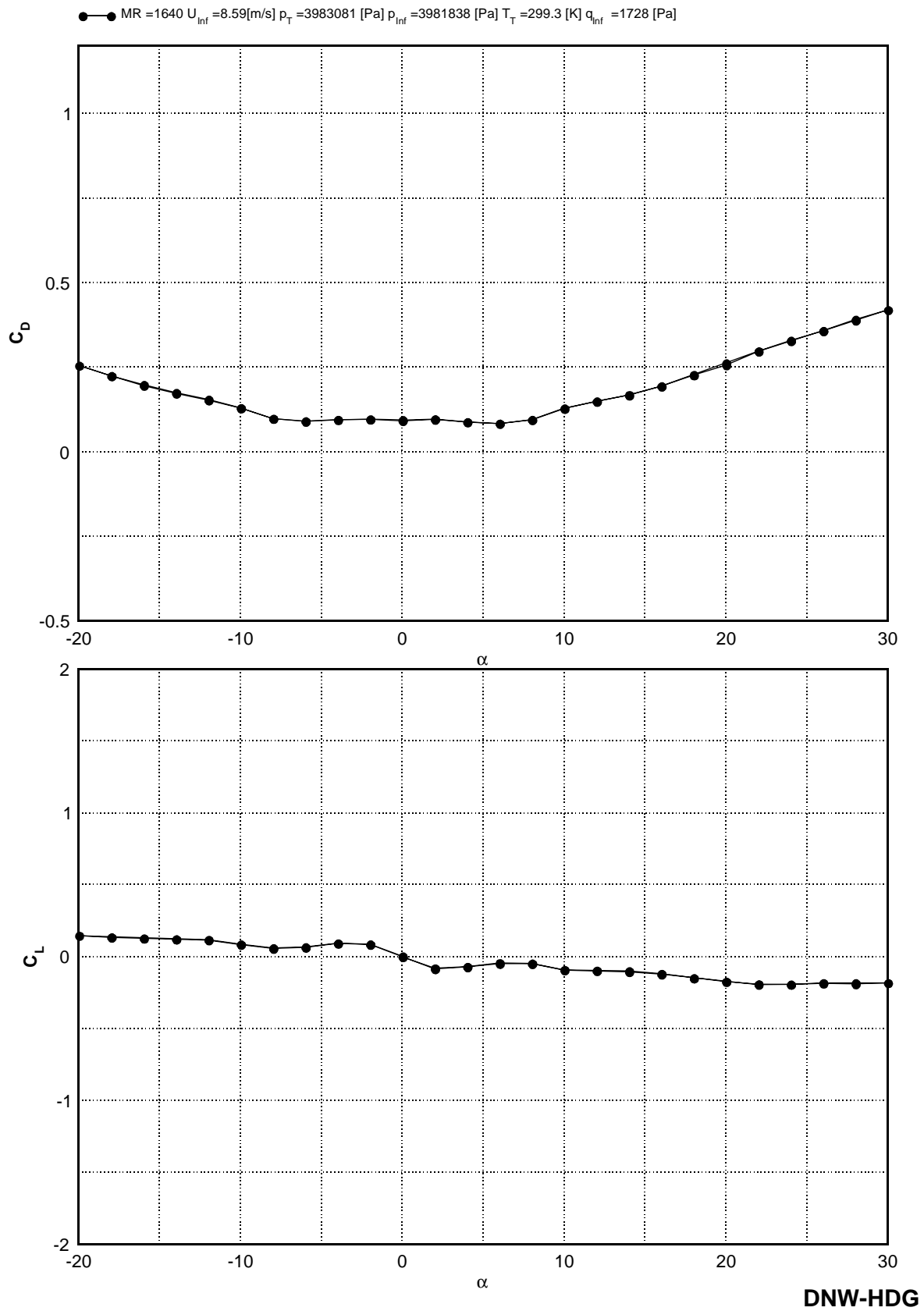


Figure 30 1<sup>st</sup> Cylinder  $Re = 1.603 [\text{Mio}]$  Pk=20bar\_vl



**Figure 31** 1<sup>st</sup> Cylinder  $Re=1.561 [\text{Mio}]$  Pk=20bar\_vl



**Figure 32** 1'st Cylinder  $Re = 0.806$  [Mio]  $Pk=40bar\_vl$



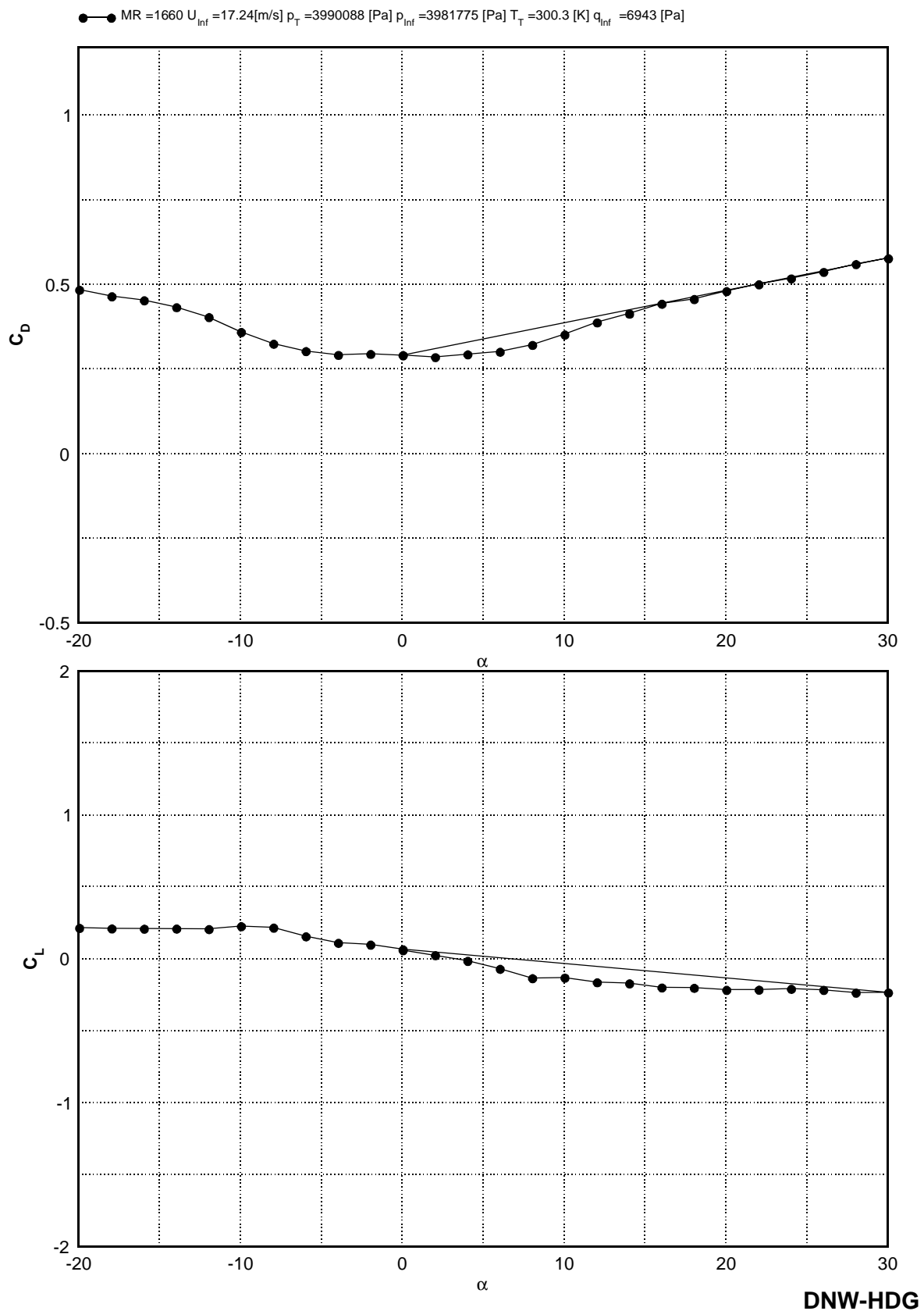
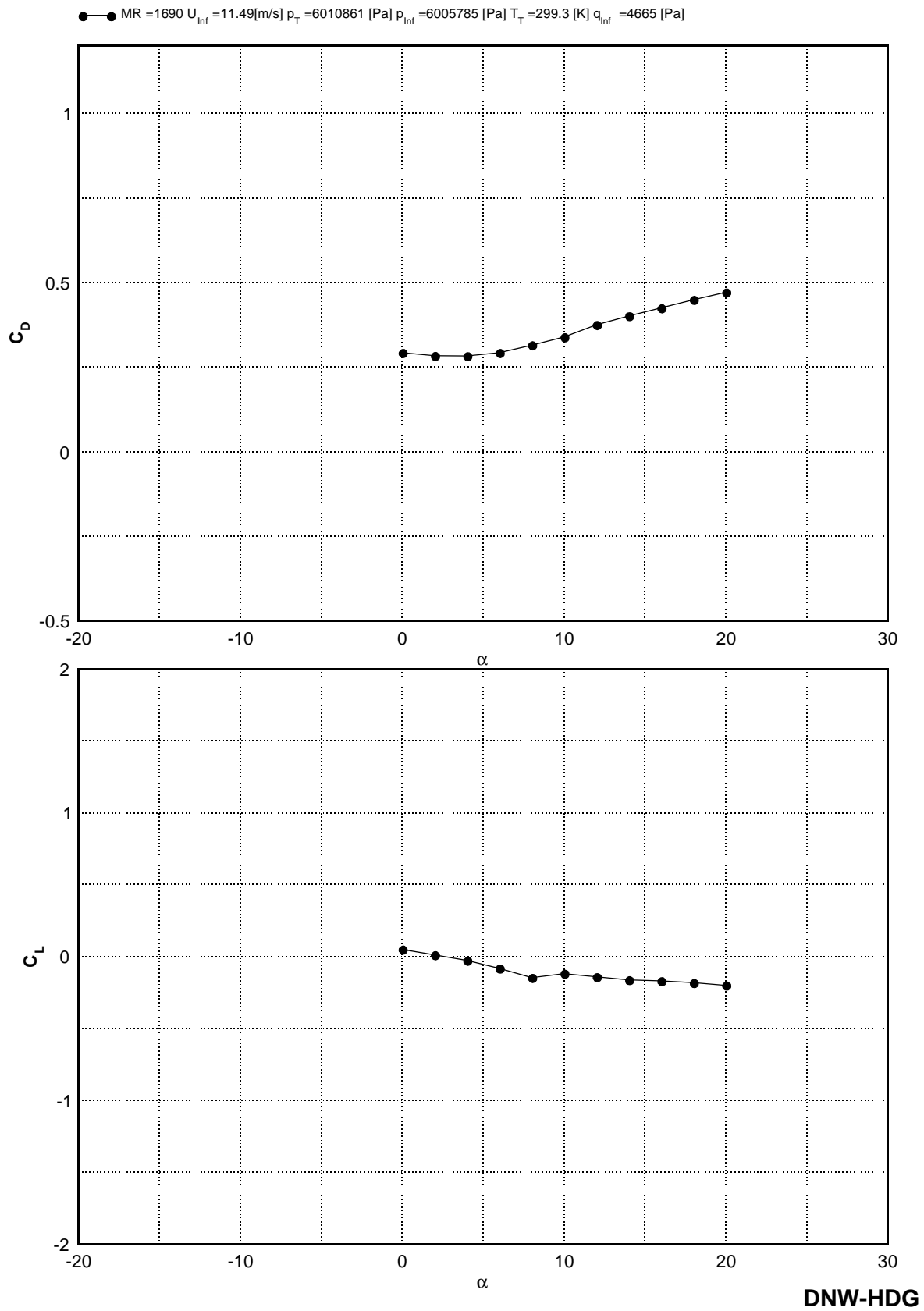


Figure 33 1'st Cylinder  $Re= 1.612 [\text{Mio}]$  Pk=40bar\_vl



**Figure 34** 1<sup>st</sup> Cylinder  $Re=1.592 [\text{Mio}]$  Pk=60bar\_vl

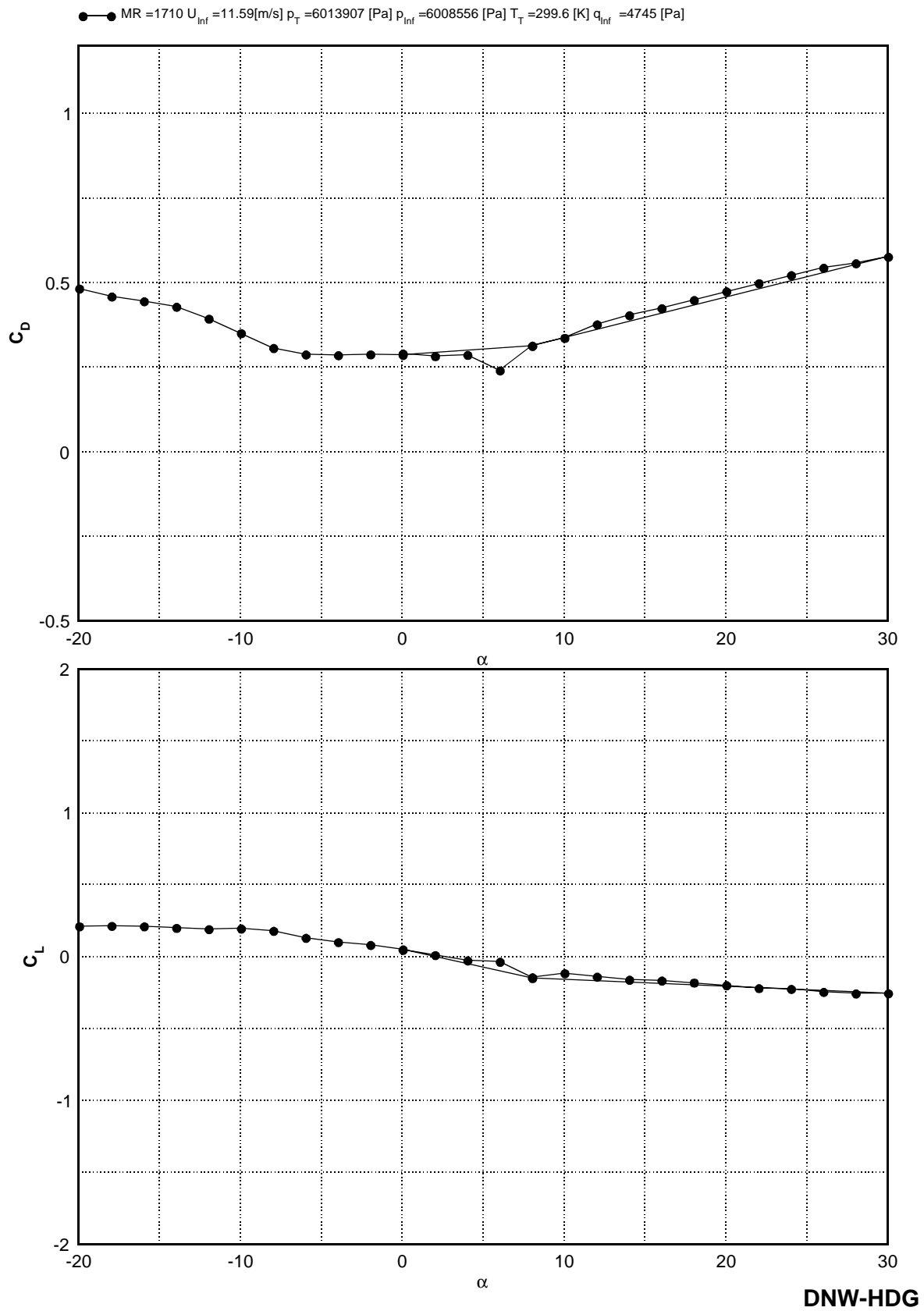


Figure 35 1'st Cylinder  $Re = 1.605 [\text{Mio}]$   $Pk = 60\text{bar\_vl}$

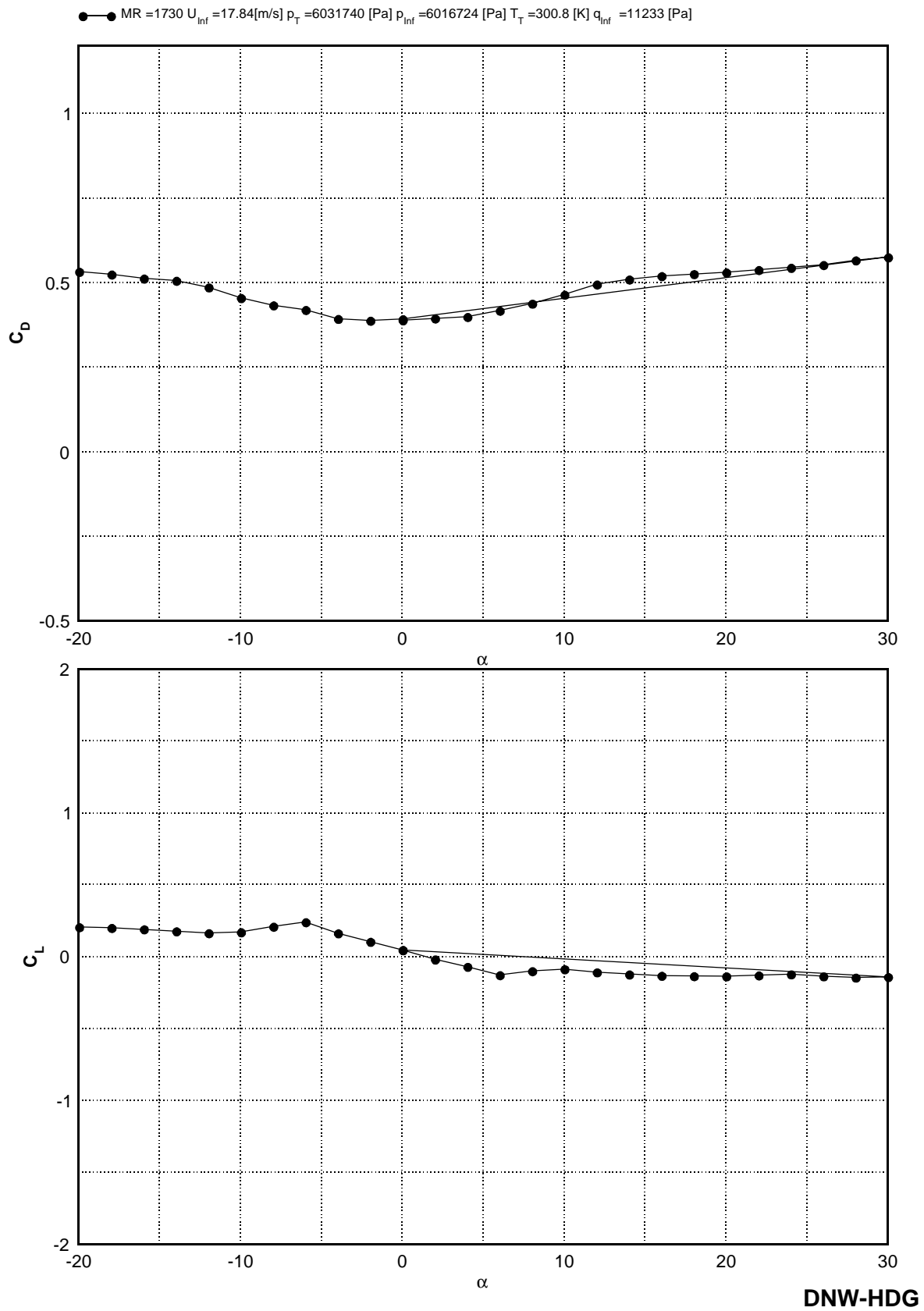


Figure 36 1'st Cylinder  $Re= 2.461 [\text{Mio}]$  Pk=60bar\_vl



